Transcriptional drifts associated with environmental changes in endothelial cells

Yalda Afshar, MD, PhD[1], Feiyang Ma, PhD[2,3], Austin Quach, PhD[2], Anhyo Jeong[1], Hannah Louise Sunshine[4,5], Vanessa Freitas, PhD[6], Yasaman Jami-Alahmadi, PhD[7], Xinmin Li, PhD[8], Matteo Pellegrini, PhD[2,3], James Wohlschlegel, PhD[6], Casey E. Romanoski, PhD[9], M. Luisa Iruela-Arispe, PhD[2,5,*]

[1]Division of Maternal Fetal Medicine, Department of Obstetrics and Gynecology, University of California, Los Angeles; [2]Department of Molecular, Cell, and Developmental Biology, University of California, Los Angeles; [3]Molecular Biology Institute, University of California, Los Angeles; [4]Department of Molecular, Cellular & Integrative Physiology, University of California, Los Angeles; [5]Department of Cell and Developmental Biology, Northwestern University Feinberg School of Medicine; Chicago, Illinois; [6]Departament of Cell and Developmental Biology, Institute of Biomedical Science, University of Sao Paulo [7]Department of Biological Chemistry, University of California, Los Angeles; ;[8]Department of Pathology and Laboratory Medicine, University of California, Los Angeles; [9]Department of Cellular and Molecular Medicine, University of Arizona, Tucson

*Corresponding author:
M. Luisa Iruela-Arispe, Ph.D.
Feinberg School of Medicine
Northwestern University
303 E. Superior Street – SQ 8-522
Chicago, IL 60611
arispe@northwestern.edu
Phone: 312-5037958

Abstract:

- Environmental cues, such as physical forces and heterotypic cell interactions play a critical role in cell function, yet their collective contributions to transcriptional changes are unclear. Focusing on human endothelial cells, we performed broad individual sample analysis to identify transcriptional drifts associated with environmental changes that were independent of genetic background. Global gene expression profiling by RNA-seq and protein expression by LC-MS directed proteomics distinguished endothelial cells in vivo from genetically matched culture (*in vitro*) samples. Over 43% of the transcriptome was significantly changed by the *in vitro* environment. Subjecting cultured cells to long-term shear stress significantly rescued the expression of approximately 17% of genes. Inclusion of heterotypic interations by co-culture of endothelial cells with smooth muscle cells normalized approximately 9% of the original *in vivo* signature. We identify novel flow depedent genes, as well as, genes that necessitate heterotypic cell interactions to mimic the *in vivo* transcriptome. Our findings highlight specific genes and pathways that rely on contextual information and physical forces.

Introduction

Endothelial cells define the functional integrity and response to hemodynamic blood forces on the luminal surface of blood vessels (1). They are also responsible for the selective trafficking of immune cells, regulation of metabolites and fluid extravasation to tissues (2-5). More recently, it has become clear that the endothelium provides instructive angiocrine signals required for the differentiation of tissues during development and for homeostasis of organs in the adult (6). In fact, it is challenging to identify a single pathological condition that could not be either worsened or improved by affecting the biology of blood vessels. Either through regulation of barrier function, anti-thrombotic properties, angiocrine or angiogenic capacity; endothelial cells have broad impact and therapeutic reach. Thus, there is a compelling incentive to define the mechanisms that control endothelial function and explore strategies to alter these functions as we work towards understanding disease etiology and processes leading to restore normal organ physiology.

Much of the knowledge accumulated on endothelial cell function has emerged through studies *in vitro*. The ability to grow endothelial cells under culture conditions has enabled investigators to identify growth factors that promote endothelial growth (7, 8), define the molecules involved in barrier function (9-11), recognize discrete steps in leukocyte-endothelial interactions (12), and much more. However, a complete reductionist *in vitro* (culture) approach deprives endothelial cells from contextual information which could impact experimental read-outs.

As for all cells, the endothelial cell transcriptome is dependent on their native environmental milieu which includes homo- and heterotypic cell interactions, soluble factors, three-dimensional organization (13), and physical forces (14-17).This contextual information is removed when cells are placed *in vitro.* While endothelial identity and many biological aspects are retained, there is no frame of reference to determine what has been lost, and what could have been artificially gained, during the transition to an *in vitro* environment. Such gains and losses are likely to affect conclusions drawn from *in vitro* expression profiles. Yet, without an understanding of these changes, the validity of conclusions associated with particular experimental challenge remains uncertain.

To gain more clarity on the impact of culture conditions on endothelial cells, we set out to evaluate human umbilical vein endothelial cells directly upon removal from the cord (*in vivo* / cord) and after exposing the same cells to short and long-term *in vitro* culture. After defining the gene signatures changed in culture, we inquired as to whether *in vitro* environmental exposure to shear stress and interactions with smooth muscle cells were able to ameliorate the differential expression signatures and “correct” drifts. Through this process and relying on genetically identical *in vivo* transcriptome, we identified groups of genes exquisitely dependent on long-term shear stress and others dependent on heterotypic cell interactions. Importantly, we also identified a large cohort of genes that were unable to regain levels comparable to *in vivo* settings and others that were artificially induced by exposure to culture conditions. Together, this work has implications for enabling investigations of endothelial cells with improved fidelity to *in vivo* phenotypes that should improve reproducibility and translation of experimental findings.

Methods

RNA isolation, quantification, and qualification:

Human umbilical cords were collected under Institutional Review Board (UCLA IRB#16-001694) at time of the delivery and processed 2-4 hours from time of birth. All samples were collected from patients who provided signed informed consent. The umbilical vein was cannulated with a 18G animal feeding needle with a blunt tip in the direction of oxygenated blood flow from the placenta to the fetus. The umbilical vein was serially washed with 20 mL of HBSS (HBBS) 3x. Subsequently, for ex-vivo samples 1mL of RLT from RNeasy Micro Kit (Qiagen, Germantown, MD), was flushed through closed circuit and re-aspirated with the distal end of the umbilical cord clamped and stored in -80-degrees C until all RNA was ready to be extraction. The length of time to obtained cells was approximately 30-60 minutes from cord clamping at delivery. For the in-vitro samples, after HBSS wash, 8 mL of collagenase-2 (210 IU, Worthington Biochemical, Lakewood, NJ) was flushed into the umbilical vein and it was incubated at 37-degrees C for 20-minutes. The flushed cells were subsequently collected and collagenase was inactivated with the addition of equivalent volume 10% feta bovine serum (FBS) with MCDB 131 media (VEC Technologies, Rensselaer, NY). The cells were pelleted, resuspended in media and plated. After cells became confluent they were passaged using 1x Trypsin (Fischer Scientific, Waltham, MA) and cells were collected with RLT for RNA extraction in early passage (passage 2-3) or late passage (passage 7-8). Subsequently all RNA was extracted concomitantly using RNeasy Micro Kit (Qiagen, Germantown, MD). Contamination with genomic DNA was eliminated with incubation of DNase I at room temperature. Agilent Bioanalyzer 2100 system (Agilent Technologies, Santa Clara, CA) was used to assess RNA integrity and Qubit (Invitrogen, Carlsbad, CA) was used for RNA concentration and purity.

Cell culture:

Primary umbilical vein endothelial cells were isolated as previously described **(18)** from umbilical cords 2-4 hours after delivery at the University of California, Los Angeles (UCLA). All HUVECs were de-identified and under UCLA IRB (IRB #16-001694). Cells were grown in culture in MCDB 131 with antibiotics (VEC Technologies, Rensselaer, NY) and containing 10% fetal bovine serum (FBS, Omega Scientific, Tarzana, CA) Cells were subsequently grown to 90-100% confluence in 10-cm^2 plates and harvested at specified passages. All primary cells were cultured tissue culture treated dishes in humidified incubator at 37°C and 5% CO_2. For co-culture experiments primary umbilical smooth muscle cells were seeded subconfluent 24h prior to seeding HUVECs at confluent density. After an additional 24h co-cultured cells were trypsinized and endothelial cells were purified using CD31 microbead kit (Miltenyi Biotec #130-091-935) according to manufacturer instructions.

Sequencing data samples and mapping:

Library preparation was performed using TruSeq Total RNASeq Kit (Illumina, San Diego, CA) according to the manufacturer's instruction. Sequencing was conducted on an Illumina HiSeq 4000 (RNAseq) and NovaSeq S2 (scRNAseq) instrument (Illumina,

San Diego, CA) at the University California Los Angeles (RNAseq, scRNAseq). Sequencing parameters were optimized for 50 bp single-end reads at a depth of 30,000 million reads/sample. Reads were mapped to the hg38 build of the human genome with Bowtie2 (19) and RNAseq reads were mapped with STAR (20). RNAseq experiments that measured accessibility and expression in different environment (cord versus culture) were all conducted at least twice. Benjamini-Hochberg false discovery rate (FDR) method was used to correct for all multiple testing in this study. No explicit power analysis was used to compute sample size.

RNAseq gene expression analysis:

Gene expression analysis was conducted using R software. First, each the log10 FPKM gene expression profile was rescaled to zero-mean and unit-resolution for both the cord vs culture and flow vs static datasets. Data was adjusted for batch effects using an empirical Bayes framework with the ComBat function from the sva package; no covariates were included in the model and the algorithm was set to use non-parametric adjustments. The expression of individuals genes was screened for associations with experimental treatments using biweight midcorrelation, a robust correlation measure, with the bicorAndPvalue function from the WGCNA package. Individual genes were also tested for associations with experimental treatments using Welch's t-test using the base R t-test function, adopting a Bonferroni-corrected significance threshold ($p < 2.5e-6$). Weighted gene co-expression network analysis was conducted using the blockwiseModulesvfunction from the WGCNA package; the network soft-thresholding power was set to 3, the network type was set to "signed hybrid"; and the entire gene set was used in for module detection by adjusting the maxBlockSize. The data can be found on the Gene Expression Omnibus (GEO) under the GEO accession number GSE158081. Both STRINGv10(21) and Metascape(22) was used to generate differential gene expression figures.

LC-MS based proteomics:

Protein samples were reduced and alkylated using 5mM Tris (2-carboxyethyl) phosphine and 10mM iodoacetamide, respectively and then digested by the sequential addition of trypsin and lys-C proteases as described (23, 24). The digested peptides were then desalted using Pierce C18 tips (Thermo Fisher Scientific, Waltham, MA), dried and resuspended in 5% formic acid, and then fractionated online using a 25cm long, 75 uM inner diameter fused silica capillary packed in-house with bulk C18 reversed phase resin (1.9 uM, 100A pores, Dr. Maisch GmbH). The 140-minute water-acetonitrile gradient was delivered using a Dionex Ultimate 3000 UHPLC system (Thermo Fisher Scientific, Waltham, MA) at a flow rate of 300 nl/min (Buffer A: water with 3% DMSO and 0.1% formic acid and Buffer B: acetonitrile with 3% DMSO and 0.1% formic acid). Peptides were ionized by the application of a distal 2.2kv and introduced into the Orbitrap Fusion Lumos mass spectrometer (Thermo Fisher Scientific, Waltham, MA) and analyzed by tandem mass spectrometry (MS/MS). Data was acquired using a Data-Dependent Acquisition (DDA) method comprised of a full MS1 scan (Resolution = 120,000) followed by sequential MS2 scans (Resolution = 15,000) to utilize the remainder of the 3 second cycle time. The mass sectrometry proteomics data have been deposited to the ProteomeXchange Consortium via the

PRIDE (25) partner repository with the dataset identifier PXD020958 and 10.6019/PXD020958. Data analysis was performed using the MSGF+ search engine (26) via the target-decoy strategy against the EMBL Human reference proteome (UP000005640 9606). The identification false detection rates (FDRs) at the peptide-spectrum-match (PSM) was defined using Percolator, protein identification confidence was estimated via the stand-alone implementation of FIDO such that analytes had respective q-values at or below 0.01 at both PSM and protein level (27-29). Extracted ion chromatograms were calculated for each peptide using Skyline (30). The MSStats R-package was used to normalize across runs using quantile normalization, summarize peptide-level intensities into a protein-level abundance, and perform statistical testing to compare protein abundance across conditions (31).

Shear stress application:
Orbital shakers were maintained in 37°C incubator with 5% CO_2. Confluent endothelial monolayers were grown on tissue culture treated 6-well plates (Falcon #08-772-1B) in complete MCDB-131 media (VEC Technologies # MCDB131-WOFBS) plus 10% FBS (Omega Scientific #FB-11) containing 4% dextran (Sigma-Aldrich #31392) for approximately 12-18 hours and then subjected to shear stress (130rpm) in new medium containing 4% dextran (Sigma-Aldrich #31392) for indicated time intervals and cultured alongside static controls. Orbital shear stress (130 rpm) was applied to confluent cell cultures by using an orbital shaker positioned inside the incubator as previously discussed (32). The shear stress within the cell culture well corresponds to arterial magnitudes (11.5 dynes/cm^2) of shear stress. To reduce issues associated with uniformity of shear stress, the endothelial cell monolayers in 6-well plates were lysed after removing center region using cell scraper (BD Falcon #35-3085) and washing with 1X HBSS (Corning #21-022-CV).

Single-cell sequencing: Single cells were isolated from umbilical cord flushes as described above. To keep the processing time between tissue harvesting and single-cell lysis at a minimum, no further cell type enrichment step was performed. For the generation of single-cell gel beads in emulsion, cells were loaded on a Chromium single cell instrument (10x Genomics, Pleasanton, CA) with an estimated targeted cell recovery of ~5,000 cells as per manufacturer's protocol. In brief, single-cell suspension of cells in 0.4% BSA-PBS were added to each channel on the 10x chip. Cells were partitioned with Gel Beads into emulsion in the Chromium instrument where cell lysis and barcoded reverse transcription of RNA occurred following amplification. Single-cell RNAseq libraries were prepared by using the Chromium single cell 3′ library and gel bead kit v3 (10x Genomics, Pleasanton, CA). Sequencing was performed (as described above) and the digital expression matrix was generated by demultiplexing, barcode processing, and gene unique molecular index counting by using the Cell Ranger pipeline (10x Genomics, Pleasanton, CA). The data can be found under the GEO accession number: GSE156939

Single-cell data analysis:
To identify different cell types and find signature genes for each cell type, the R package Seurat (version 3.1.2) was used to analyze the digital expression matrix. Cells

with less than 500 unique molecular identifiers (UMIs) and greater than 50% mitochondrial expression were removed from further analysis. Seurat function NormalizeData was used to normalize the raw counts. Variable genes were identified using the FindVariableGenes function; genes with normalized expression values between 0.1 and 5 and with a dispersion of at least 0.5 were considered variable. The Seurat ScaleData function was used to scale and center expression values in the dataset for dimensional reduction. Principal component analysis (PCA), *t*-distributed stochastic neighbor embedding (t-SNE), and uniform manifold approximation and projection (UMAP) were used to reduce the dimensions of the data, and the first 2 dimensions were used in plots. A graph-based clustering approach was later used to cluster the cells; then signature genes were found and used to define cell types for each cluster. ECs were selected based on high expression of *PECAM1* and *CDH5* genes. SMCs were identified by the high expression of *ACTA2* and *TAGLN* genes. Module scores were calculated using the AddModuleScore function with default parameters.

Results

To uncover changes on endothelial cells as result of exposure to culture conditions, we evaluated the transcriptome of endothelial cells isolated from human postnatal umbilical veins. Half of each patient's cell preparation was freshly processed for RNA isolation (referred to as "cord") while the other half was placed under culture conditions (referred to as "culture"). Cells were subsequently passaged and evaluated at early passage (P 2-3) and late passage (P 7-8) to capture transcriptional differences between cellular environments that were common amongst all seven patients regardless of fetal sex or genetic background (Figure 1a, Supplemental Excel 1). Patient demographics with paired maternal-fetal outcomes are provided in Table 1, and each patient had matched cord, early passage, and late passage paradigm. Principal component analysis (PCA) of bulk RNA sequencing (RNAseq) transcriptional profiles revealed that cord versus in vitro environments were the dominant factor influencing measured expression levels (Figure 1b-c). PC1 captured 47.4% of the total variance whereas PC2 only accounts for 11.1%. Interestingly, PC2 appears to represent the differences between early and late passage but these conditions did not segregate from each other as clearly as cord versus in vitro culture.

Approximately half of the genes were differentially expressed between cord and culture conditions (4,532-4,645 genes overlapping), whereas the transcriptomic signature was very similar between early and late culture (11,706 genes overlapping) (Figure 1d). As such, we considered only differences between cord and culture signatures going forward (Figure 1e-g, Supplemental Excel 1, Supplemental Figure 1).

Genes with robust changes in expression are highlighted in Figure 1e-f. Amongst several signatures, we observed that TGF-beta and BMP target genes were reduced under culture. Some of the most *in vivo*-specific transcripts were related to the extracellular matrix; while several genes specific to the *in vitro* environment associated with the cell cycle (Supplemental Excel 1). We also found that the most highly expressed genes across patients and environments demonstrated minimal variation across individuals and considerable variation between environments (Supplemental Excel 1, Figure 1f). As expected, we found that endothelial cells lose expression of flow-

responsive genes (*KLF4, KLF2*) once placed under culture conditions, whereas they quickly acquire proliferative-related genes (*CCNB2, CCNA2, CDCA2*). Perhaps more surprising was that transition into culture promotes a significant decrease in transcripts associated with extracellular matrix genes (*COL23A1, MMP28, FBLN2, ELN, COL1A2, COL6A3*), cytokine (*CXCL2, SOCS3*, *TGFB3, CTGF*), and early response genes (*FOS, ZFP36, JUNB*) (Supplemental Excel 1). In addition to increased expression of cell cycle genes in culture, transcripts associated with survival and a pro-angiogenic phenotype were also upregulated (e.g., *APLN, BAX, CCN*, *CCNB2, CCNBA1, CEPH1, CDCA7l, CDCA2, MDM2*). Further, the significant increase of VEPH1 under culture conditions was of particular interest as this protein product of this gene is associated with suppression of TGFß1, FOXO and Wnt signaling (33).

Gene Ontology term enrichment of differentially expressed genes was performed using GO biological processes. Significant terms, defined using hypergeometric p-values and enrichment factors, were then hierarchically clustered based on similarities among gene members into networks (Figure 1g; see Methods). In the network, terms are represented by a node with its size proportional to the number of differentially expressed genes in that term. Focusing on genes expressed uniquely in cord relative to culture, we found enrichment of genes with documented involvement into blood vessel development, skeletal system development (mostly the TGFß family), heart / blood vessel development, ossification (extracellular matrix genes), and cytokine production (Figure 1g).

To determine whether the identified changes were supported by similar drifts at the protein level, validation of the transcriptomic signature was performed by comparing cord and *in vitro* protein extracts by untargeted LC-MS based proteomics. PCA analysis of relative protein abundances was performed for seven matched individuals from the cord and early culture, demonstrate clear separation of the experimental conditions (Figure 1h and Table 1). In agreement to the RNA level differences, there were significant changes in protein expression between the environments. Albeit not as remarkably different than the transcriptomic read-outs (likely due to depth of coverage and statistical power), we identified an -omics signature of proteins specific to cord (about 160/3000 proteins) and to early culture (about 411/3000 proteins) (Supplemental Figure 1e). These differences are clearly noted in Supplemental Figure 1f.

To explore the degree of overlap between RNA and protein, we compared the results of differential transcripts using the cord *versus* culture analysis to that of protein cord *versus* culture analysis (Supplemental Figure 1g). The relationships between t-statistics between cord and culture across -omic layers revealed significant correlation between RNA and protein signatures ($r=0.4$, $p=1x10^{-07}$) (Figure 1i). Consistent with prior findings, the data revealed low expression of cell cycle proteins and high expression of flow-responsive proteins in the cord (ex-vivo) proteomics profile (Figure 1i, Supplemental Excel 2).

As a large number of genes associated with transition from cord to culture appeared to be flow-related, we explored the potential to ameliorate these differences by imposing shear stress on cultured cells. This approach is warranted by observations that once placed under laminar flow, endothelial cells elongate in the direction of flow in a similar morphology than *in vivo* (34). Further, the onset of flow is associated with significant transcriptional increase in flow responsive genes, like *KLF2* (35-37), which is

one of the cord-specific transcripts (Figures 1,2). We thus performed two comparisons: 1) static culture to flow cultures, and, 2) each to cord endothelial cells (Figures 2,3).

Shear stress significantly rescued the expression of approximately 17% of genes including targets of BMP and Notch signaling known to be sensitive to flow. At the transcriptional level, the effect of physical forces, particularly laminar, oscillatory and turbulent flow have been extensively investigated (38-41). These investigations have been instrumental to clarify the effect of shear stress on endothelial cells. The large majority of the studies, however, focused on early responses to flow conditions and missed comparisons to cells immediately removed from the vessel that could offer a frame of reference for the *in vivo* state. We took advantage of having isolated cells directly from the cord and compared their transcriptome to the genetically identical progeny subjected to static and laminar flow conditions over time.

First, principal component analysis of matched patients (n=4, Table 1) demonstrated static cells *in-vitro* and under 30-minutes of flow had a relatively similar global transcriptional signatures. Differences were apparent on PC1 with flow, defined as 8-48 hours of laminar shear stress exposure (Figure 2b). Figure 2c provides a clear delineation and transcriptomic signature as a function of static (control and 30min) versus longer time points (8, 24, 48hr of flow). Significant changes (log10FC) were noted between static and flow cultures (Figure 2d and Supplemental Excel 3-4), with *IGFBP5, ELN, KLF4, ETPR1*, and *TGFBR3* significantly dependent on flow for the transcriptional increase. Correlation scatter plots of the cord versus culture (x-axis) were compared to time under flow (y-axis) and this analysis showed a time-dependent positive correlation to the cord transcriptome (vs culture) (Figure 2e). Progressive time under flow from up to 48-hours of shear stress (flow) revealed that the transcriptional signature of cells correlates more specifically to that of the cord than with static cultures. Initially, the correlation coefficient was insignificant (r=-0.035, p=0.004) with progressive changes to the point that by 48-hours of shear stress the correlational coefficient to cord reaches r=0.34, =-8.0x10^{-9}, which is significantly different than static culture (Figure 2e). Collectively these data offer proof that drifts in the transcriptome of endothelial cells under culture can be partially rescued by exposure to laminar shear stress.

A marked change towards the cord state was noted also by pathway analysis. Specifically GO terms associated with blood vessel development (*EDN1, BMP2, BMP4, TGFPR3, ITG1BP1, HES1, HEY1*), regulation of cellular protein location (*ITGA3, RACK1, PTPN9, SPTBN1*), and cellular response to laminar fluid shear stress (*ASS1, KLF2, KLF4, MAPK7, NFE2L2*) were regained by long-term exposure to flow (Figure 2f). Gene set enrichment analysis of differential genes in cultured endothelial cells under flow (versus static) revealed gene annotations related to an acute inflammatory response, heart morphogenesis, second messenger-mediated signaling, and ossifications. We also found tRNA and rRNA metabolic processes were silenced under flow (Supplemental Figure 2-3, Supplemental Excel 3-4).

Superimposing the cord and culture signatures (from Figure 1) with the static versus flow experiments (from Figure 2) clarifies how the transcriptional profile of cultured cells under flow approximates to better to the *in vivo* transcriptome when compared to static states (Figure 3a, across PC1). This shift was also noted by evaluating total number of transcriptional changes up or downregulated (Figure 3b). In fact, much of the cord signature overlapped with genes that were rescued or attenuated

under flow and paralleled those expressed by the cord. Specifically, the incorporation of shear stress to the *in vitro* static conditions attenuated the variability between cord and culture (Figure 3).

To begin to identify genes and networks that approximate the *in vivo* environment and are conveyed by long-term exposure to shear stress, we performed a transcriptome-wide weighted gene co-expression network analysis (WGCNA). This approach led us to identify 36 co-expression modules, revealing gene groups that are co-enriched in either cord or culture environments, in static versus flow conditions (Figure 3c, red: down; blue: up), and to patient-level WGCNA (Supplemental Excel 3-4, Supplemental Figure 3). Relative expression values for the most expressed modules across each of the patients are illustrated in Supplemental Figure 3d-e and then culminated in summary in Figure 3d.

Superimposing the cord transcriptome on the flow transcriptome, highlighted co-expressed modules with significant enriched directionality in cord and culture transcriptomes (Figure 3c). Gene ontology (GO) network analysis of WGCNA demonstrated that differential modules were selectively increased (blue) and decreased (brown) by long-term exposure to shear stress (Figure 3e). The blue (2,185 genes, r=0.71, p=3e-04) module showed increased transcriptional concurrence with the cord and this was progressive with time under flow (r=0.8, p=4e-04). Although exposure to shear stress partially recapitulated the cord environment (Figure 3e), this was not the case for all the transcripts, highlighting signatures that are exquisitely flow-dependent and others that are flow-independent and likely regulated by alternative factors, such as heterotypic cell interactions. Notably, the genes and GOs associated with this module included blood vessel development and leukocyte activation (Figure 3f). The brown module (1,408 genes, r=-0.9, p=3e-08), defined by cell cycle and cell cycle checkpoints, was less expressed in cord (vs culture) and in flow (vs static, r=-0.62, p=0.01). These genes gained expression in culture, yet flow reverted their phenotype to more low expression as was evident in cord (Figure 3g-h, Table 2-3, Supplemental Excel 5). In summary, this network analysis uncovered co-expressed gene signatures that are sensitive to shear stress (induced, aka blue module and repressed, aka brown module) and represented in vivo.

Given these global differences between cord and culture, we asked whether this differential gene expression was also affected by heterotypic cell interactions, namely with smooth muscle cells. To address this question, we leveraged single cell RNA sequencing (scRNAseq) technology to obtain transcriptomes of individual cells isolated from endothelial cells in a homogenous culture versus endothelial cells co-cultured with smooth muscle cells (co-culture, CC). The approach was aimed at further approximating contextual environment and obtain signatures responsive to those changes (Figure 4a). We profiled triplicates of primary endothelial cells, primary smooth muscle cells (mono-cultures), and co-cultured endothelial cells and smooth muscle cells all plated to confluency using scRNAseq (Supplemental Excel 6, Supplemental Figure 4). Endothelial and smooth muscle cells were isolated from the same cord. In total, 51,000 cells were sequenced with an average of 3,402 genes and 18,740 transcripts per cell. Individual samples were independently analyzed to confirm correlation between triplicates, normalized and then combined for analysis. Unsupervised clustering demonstrated the cells cluster by origin (Figure 4b-e). We then confirmed cell clusters

as endothelial cells (*PECAM1* and *CDH5*, Figure 4c-e) and smooth muscle cells (*ACTA2* and *TAGLN*) (data not shown).

Transcriptomic profiles that defined each cluster was performed by Seurat and this information offered initial insight on transcriptional shifts that occurred as a consequence to heterotypic cell interactions. As shown by heatmap (Figure 4f), clear differences were noted when endothelial cells were in mono-culture (MC) versus co-culture (CC). Specifically, co-culture prompted a reduction in NOTCH target genes (*FABP4, GJA4, FABP5, HEY*) and a clear induction in TGFß downstream targets (*SERPINE1, IGFBP7, SOX4, TIMP1*) (Figure 4f). Ingenuity pathway analysis provided further clarification as to the functional impact related to presence of smooth muscle cells. As shown in Figure 4g, the major signaling pathways and transcriptional regulators that prompted transcriptional drifts on endothelial cells by co-culture included TGFß, VEGF, TP53, HTT, MYC, TNF, EDN1, SP1 and HGF. We calculated a module score using the expression of downstream targets for TFGß1 and VEGFA identified by ingenuity pathway analysis, and found a significant increase upon co-culture for both (Figure 4h). This is to be expected as smooth muscle cells provide a source for these those two cytokines. This results in shifts in extracellular matrix proteins, MMPs, and integrins (Figure 4i) and it is further supported by transcriptional increases in TGFß receptors ACVRL1 and ENG. Interestingly, co-culture conditions resulted in an increase of clathrin-related genes (*AAK1, AP2B1* and *CLTB*) and a decrease in caveolin-related genes (*CAV1* and *CAV2*) (Figure 4j). These changes occurred with no significant alterations in *CDH5, ERG, NOTCH1* and *JAG1* (Figure 4k).

Naturally the next question focused on which signatures impacted by heterotypic cell interactions yield a rescue of the *in vivo* condition. To delineate these transcriptional relationships, we overlapped scRNA sequencing data obtained from cord-derived endothelial cells and compared them to the mono and co-culture endothelial transcriptomes (Figure 5a-c, Supplemental Excel 7-8). Interestingly, global transcriptional profiling in UMAP showed a shift of co-culture towards cord (Figure 5a). In-depth analyses of the data using Seurat, GOs and ingenuity pathways reveals cohorts of genes that were indeed rescued (either up or down-regulated) and also genes that were not rescued by the co-culture condition. Examples of those categories are shown in Figure 5d and group analysis by dot blot as displayed in Figure 5e. Genes rescued by co-culture relate to NOTCH signaling (*HES1, FABP4*) and TGFß (*ENG*). In addition, we found that clathrin pathways, noted to be increased by SMC-co-culture (Figure 4) were indeed part of the *in vivo* signature displayed by endothelial cells in the cord (Figure 5f) with upregulation of transcripts for *AAK1* and *EPN2*. Co-culture also was responsible for rescue of TJP1, responsible for tight junctions and two transmembrane proteins that regulate calcium homeostasis (TMEM165 and 203) (Figure 5f). Interestingly we noticed a decreased in *IRF7* and *VASH1* under co-culture that also approximated the cord condition.

In summary, co-culture of endothelial cells with smooth muscle cells normalized networks related to cell growth and differentiation, clathrin-vesicle related genes, and recovered targets downstream TGF-beta, recovering approximately 9% of the original cord (*in vivo*) signature.

Discussion

Endothelial cells are characterized by a unique set of genes collectively referred to identity genes (i.e. *CDH5, PECAM1, ERG*) and a group of genes whose expression levels varies according to stressors and environmental conditions. Precise information of both groups holds relevance to the interpretation of findings related to any experimental challenge. Despite the broad utilization of cultured endothelial cells, drifts in the transcriptional profiles upon expansion *in vitro* have not been rigorously addressed. Here, we undertook parallel transcriptomics analyses using genetically identical matches to determine the impact of the environment of cell culture and define whether specific signatures could be regained by changing environmental settings that will best approximate the native biological state.

To minimize confounding factors related to intrinsic genetic differences, we performed parallel transcriptomic profiling. Seven pairs of freshly isolated *versus* cultured endothelial cells were used for the initial profiles and the findings from these were validated against proteomics from seven independent pairs. Four additional cohorts were used to compare static *versus* flow *versus* freshly isolated conditions and single-cell RNAseq was subsequently used in the co-culture experiments. Our findings highlighted signatures that were uniquely associated with long-term exposure to shear stress *in-vitro* that parallel expression profiles *ex-vivo*. We also identified signatures dependent on heterotypic, endothelial-smooth muscle cell interactions that were lost *in-vitro*, but a hallmark of the *ex-vivo* state. The findings offer an important resource to query how expression profiles of specific genes change in relation to a subset of environmental conditions.

A major adaptation that cells must acquire when placed in culture relates to cell proliferation. Once seeded, endothelial cells undergo significant expansion that is thought to be attenuated or suppressed at confluency. Nonetheless, we demonstrate that high levels of transcripts related to cell cycle, mitosis, and DNA repair mechanisms are still present at confluency and represent the single most significant alteration when comparing freshly isolated cells to genetically identical cohorts *in vitro*. Similarly, there are significant alterations in cytoskeleton dynamics and focal adhesions that are artificially elevated *in vitro*, compared to *ex-vivo*.

Recapitulating the native flow seen by endothelial cells by exposure of static cultures to shear stress resulted in a significant shift towards ex vivo (freshly isolated cells) signature. Much has been done to understand transcriptional responses to flow most of these have been focused on early responses in the absence of *in vivo* genetically-matched counterparts (42-47). Our data found agreement with previous findings of short time exposure to shear stress, in particular, we noted an impressive induction of KLF2 and KLF4 (48). However, longer exposure to laminar flow (8, 24, 48hrs) progressively increased the resemblance to the *ex vivo* transcriptome, as noted by correlation coefficients. Specifically, we found that two major pathways and their downstream genes were regained by long-term flow: BMP and NOTCH signaling. Importantly, it has been recently shown that BMP signaling is significantly potentiated by flow (49). Indeed, several SMAD targets were rescued by incorporating long-term flow into cultures. Similarly, NOTCH target genes (*HES, HEY*) regained levels similar to

those captured in freshly isolated preparations. These findings are congruent with recent studies demonstrating that NOTCH signaling was increased by flow (50). An unexpected gene ontology signature regained by shear stress were proteins associated with cellular localization, such as ITPR1, IGFBP5, DLL1, among others, highlighting the role of laminar shear stress in endothelial cell polarity.

Alterations in junctional proteins and cytoskeletal architecture were recovered in endothelial-smooth muscle cell co-cultures. The co-culture of smooth muscle cells also TGF-beta downstream targets, including several extracellular matrix proteins and integrins which bring further alignment to the *in vivo* transcriptome. In addition, smooth muscle cells significantly reduced the prominent proliferative signature of endothelial cells and promoted a partial recovery in endothelial cell differentiation. Specifically, this included ENG as well as integrins regulated by TGFß1 (ITGB1, ITGA1, ITGA5), as well as several extracellular membrane proteins (COL1A1, FN1, TIMP1, SERPINE1) (51-53). It can be postulated that loss of architecture in-vitro could induce the loss of expression of acute phase transcripts, as seen with injury of the aorta *in vivo* (54). These endothelial-heterotypic crosstalks have been shown essential during development and vascular pathologies such as aneurysms (55).

Exposing endothelial cells to culture conditions does not appear to significantly affect cellular identity. Transcriptional levels of CDH5, PECAM1, ERG, Claudins, Sox(s), and other so-called endothelial markers were not significantly impacted. ERG is essential for regulation of CDH5, VWF, and NOS3 as well as for endothelial cell lineage (56-60).

The ability to grow and study endothelial cells *in vitro* has enabled investigators to ask questions under well controlled, yet artificial, conditions. The consequences associated with phenotypic alterations of ex vivo expanded cells remain unknown despite ample evidence that culture conditions exert profound influence upon cellular biological properties (61-64). We defined a transcriptionally unique fingerprint of endothelial cells immediately removed from the cord and mapped how environmental changes uniquely impact this profile. These -omics analyses offer information that will guide researchers to have a better understanding of intrinsic mechanisms that are not captured when studying signaling pathways and molecular processes in culture. Appreciating these nuances and recapitulating intrinsic shear stress and heterotypic cell interactions will help propel reprogramming efforts for the generation of a more representative *in vivo* model system *in vitro* and allow us to better interpret genetic modifiers that affect or are affected by endothelial cells.

Author contributions: Y.A. contributed to the conception, design, acquisition, interpretation of the data, and drafted the manuscript. F.M. contributed to the analysis and interpretation of the data. A.Q. contributed to the analysis and interpretation of the data. H.S. contributed to the acquisition of the data V.F. contributed to the acquisition of the data. A.J. contributed to the acquisition of the data. Y.J. contributed to the acquisition of the data. X.L. contributed to the acquisition of data. M.P. supervised F.M. in the analysis and interpretation of the data. J.W. contributed to the interpretation of the data. C.R. contributed to the design, acquisition, and interpretation of the data. M.L.I.A contributed to the conception, design, interpretation of the data, and drafted the manuscript. All authors (Y.A., F.M., A.Q., V.F., A.J., Y.J, X.L., M.P., J.W., C.R., and M.L.I.) have approved the submitted version and agreed to be accountable for the author's own contribution and to ensure that questions related to the accuracy or integrity of any part of the work, even ones in which the author was not personally involved, are appropriately investigated, resolved, and the resolution documented in the literature.

Acknowledgments: This work was supported by a grant from the National Institutes of Health R35HL140014 (M.L.I.A), R01HL147187 (C.E.R.), FAPESP 2016/19968-3 (V.F.), and K12 HD000849 (Y.A.), awarded to the Reproductive Scientist Development Program by the Eunice Kennedy Shriver National Institute of Child Health & Human Development, by the March of Dimes and American College of Obstetricians and Gynecologists, as part of the Reproductive Scientist Development Program (Y.A.), and the Ruth L. Kirschstein National Research Service Award T32HL069766 (Y.A.).

References

1. Iruela-Arispe ML, Davis GE. Cellular and molecular mechanisms of vascular lumen formation. Dev Cell. 2009;16(2):222-31.
2. Jackson DG. Leucocyte Trafficking via the Lymphatic Vasculature- Mechanisms and Consequences. Front Immunol. 2019;10:471.
3. Sun X, Feinberg MW. Regulation of endothelial cell metabolism: just go with the flow. Arterioscler Thromb Vasc Biol. 2015;35(1):13-5.
4. Vandenbroucke E, Mehta D, Minshall R, Malik AB. Regulation of endothelial junctional permeability. Ann N Y Acad Sci. 2008;1123:134-45.
5. Wettschureck N, Strilic B, Offermanns S. Passing the Vascular Barrier: Endothelial Signaling Processes Controlling Extravasation. Physiol Rev. 2019;99(3):1467-525.
6. Gomez-Salinero JM, Rafii S. Endothelial cell adaptation in regeneration. Science. 2018;362(6419):1116-7.
7. Apte RS, Chen DS, Ferrara N. VEGF in Signaling and Disease: Beyond Discovery and Development. Cell. 2019;176(6):1248-64.
8. Gerber HP, Dixit V, Ferrara N. Vascular endothelial growth factor induces expression of the antiapoptotic proteins Bcl-2 and A1 in vascular endothelial cells. J Biol Chem. 1998;273(21):13313-6.
9. Christensen PM, Liu CH, Swendeman SL, Obinata H, Qvortrup K, Nielsen LB, et al. Impaired endothelial barrier function in apolipoprotein M-deficient mice is dependent on sphingosine-1-phosphate receptor 1. FASEB J. 2016;30(6):2351-9.
10. Corada M, Orsenigo F, Bhat GP, Conze LL, Breviario F, Cunha SI, et al. Fine-Tuning of Sox17 and Canonical Wnt Coordinates the Permeability Properties of the Blood-Brain Barrier. Circ Res. 2019;124(4):511-25.
11. Trani M, Dejana E. New insights in the control of vascular permeability: vascular endothelial-cadherin and other players. Curr Opin Hematol. 2015;22(3):267-72.
12. Muller WA. Transendothelial migration: unifying principles from the endothelial perspective. Immunol Rev. 2016;273(1):61-75.
13. Wang S, Wang B, Shi Y, Moller T, Stegmeyer RI, Strilic B, et al. Mechanosensation by endothelial PIEZO1 is required for leukocyte diapedesis. Blood. 2022.
14. Choi JS, Seo TS. Orthogonal co-cultivation of smooth muscle cell and endothelial cell layers to construct in vivo-like vasculature. Biomicrofluidics. 2019;13(1):014115.
15. Cleuren ACA, van der Ent MA, Jiang H, Hunker KL, Yee A, Siemieniak DR, et al. The in vivo endothelial cell translatome is highly heterogeneous across vascular beds. Proc Natl Acad Sci U S A. 2019;116(47):23618-24.
16. Dayang EZ, Plantinga J, Ter Ellen B, van Meurs M, Molema G, Moser J. Identification of LPS-Activated Endothelial Subpopulations With Distinct Inflammatory Phenotypes and Regulatory Signaling Mechanisms. Front Immunol. 2019;10:1169.
17. Jambusaria A, Hong Z, Zhang L, Srivastava S, Jana A, Toth PT, et al. Endothelial heterogeneity across distinct vascular beds during homeostasis and inflammation. Elife. 2020;9.

18. Crampton SP, Davis J, Hughes CC. Isolation of human umbilical vein endothelial cells (HUVEC). J Vis Exp. 2007(3):183.
19. Langmead B, Salzberg SL. Fast gapped-read alignment with Bowtie 2. Nat Methods. 2012;9(4):357-9.
20. Dobin A, Davis CA, Schlesinger F, Drenkow J, Zaleski C, Jha S, et al. STAR: ultrafast universal RNA-seq aligner. Bioinformatics. 2013;29(1):15-21.
21. Szklarczyk D, Franceschini A, Wyder S, Forslund K, Heller D, Huerta-Cepas J, et al. STRING v10: protein-protein interaction networks, integrated over the tree of life. Nucleic Acids Res. 2015;43(Database issue):D447-52.
22. Zhou Y, Zhou B, Pache L, Chang M, Khodabakhshi AH, Tanaseichuk O, et al. Metascape provides a biologist-oriented resource for the analysis of systems-level datasets. Nat Commun. 2019;10(1):1523.
23. Wohlschlegel JA. Identification of SUMO-conjugated proteins and their SUMO attachment sites using proteomic mass spectrometry. Methods Mol Biol. 2009;497:33-49.
24. Florens L, Carozza MJ, Swanson SK, Fournier M, Coleman MK, Workman JL, et al. Analyzing chromatin remodeling complexes using shotgun proteomics and normalized spectral abundance factors. Methods. 2006;40(4):303-11.
25. Perez-Riverol Y, Csordas A, Bai J, Bernal-Llinares M, Hewapathirana S, Kundu DJ, et al. The PRIDE database and related tools and resources in 2019: improving support for quantification data. Nucleic Acids Res. 2019;47(D1):D442-D50.
26. Kim S, Pevzner PA. MS-GF+ makes progress towards a universal database search tool for proteomics. Nat Commun. 2014;5:5277.
27. Serang O, MacCoss MJ, Noble WS. Efficient marginalization to compute protein posterior probabilities from shotgun mass spectrometry data. J Proteome Res. 2010;9(10):5346-57.
28. Granholm V, Kim S, Navarro JC, Sjolund E, Smith RD, Kall L. Fast and accurate database searches with MS-GF+Percolator. J Proteome Res. 2014;13(2):890-7.
29. The M, MacCoss MJ, Noble WS, Kall L. Fast and Accurate Protein False Discovery Rates on Large-Scale Proteomics Data Sets with Percolator 3.0. J Am Soc Mass Spectrom. 2016;27(11):1719-27.
30. MacLean B, Tomazela DM, Shulman N, Chambers M, Finney GL, Frewen B, et al. Skyline: an open source document editor for creating and analyzing targeted proteomics experiments. Bioinformatics. 2010;26(7):966-8.
31. Choi M, Chang CY, Clough T, Broudy D, Killeen T, MacLean B, et al. MSstats: an R package for statistical analysis of quantitative mass spectrometry-based proteomic experiments. Bioinformatics. 2014;30(17):2524-6.
32. Dardik A, Chen L, Frattini J, Asada H, Aziz F, Kudo FA, et al. Differential effects of orbital and laminar shear stress on endothelial cells. J Vasc Surg. 2005;41(5):869-80.
33. Shathasivam P, Kollara A, Ringuette MJ, Virtanen C, Wrana JL, Brown TJ. Human ortholog of Drosophila Melted impedes SMAD2 release from TGF-beta receptor I to inhibit TGF-beta signaling. Proc Natl Acad Sci U S A. 2015;112(23):E3000-9.
34. Chiu JJ, Chien S. Effects of disturbed flow on vascular endothelium: pathophysiological basis and clinical perspectives. Physiol Rev. 2011;91(1):327-87.
35. Chien S. Mechanotransduction and endothelial cell homeostasis: the wisdom of the cell. Am J Physiol Heart Circ Physiol. 2007;292(3):H1209-24.

672 36. Nakajima H, Mochizuki N. Flow pattern-dependent endothelial cell responses
673 through transcriptional regulation. Cell Cycle. 2017;16(20):1893-901.
674 37. Zhou J, Li YS, Chien S. Shear stress-initiated signaling and its regulation of
675 endothelial function. Arterioscler Thromb Vasc Biol. 2014;34(10):2191-8.
676 38. Kim CW, Pokutta-Paskaleva A, Kumar S, Timmins LH, Morris AD, Kang DW, et
677 al. Disturbed Flow Promotes Arterial Stiffening Through Thrombospondin-1. Circulation.
678 2017;136(13):1217-32.
679 39. Nakajima H, Yamamoto K, Agarwala S, Terai K, Fukui H, Fukuhara S, et al.
680 Flow-Dependent Endothelial YAP Regulation Contributes to Vessel Maintenance. Dev
681 Cell. 2017;40(6):523-36 e6.
682 40. Peng Z, Shu B, Zhang Y, Wang M. Endothelial Response to Pathophysiological
683 Stress. Arterioscler Thromb Vasc Biol. 2019;39(11):e233-e43.
684 41. Polacheck WJ, Kutys ML, Yang J, Eyckmans J, Wu Y, Vasavada H, et al. A non-
685 canonical Notch complex regulates adherens junctions and vascular barrier function.
686 Nature. 2017;552(7684):258-62.
687 42. Ajami NE, Gupta S, Maurya MR, Nguyen P, Li JY, Shyy JY, et al. Systems
688 biology analysis of longitudinal functional response of endothelial cells to shear stress.
689 Proc Natl Acad Sci U S A. 2017;114(41):10990-5.
690 43. Chen BP, Li YS, Zhao Y, Chen KD, Li S, Lao J, et al. DNA microarray analysis of
691 gene expression in endothelial cells in response to 24-h shear stress. Physiol
692 Genomics. 2001;7(1):55-63.
693 44. Chu TJ, Peters DG. Serial analysis of the vascular endothelial transcriptome
694 under static and shear stress conditions. Physiol Genomics. 2008;34(2):185-92.
695 45. Conway DE, Williams MR, Eskin SG, McIntire LV. Endothelial cell responses to
696 atheroprone flow are driven by two separate flow components: low time-average shear
697 stress and fluid flow reversal. Am J Physiol Heart Circ Physiol. 2010;298(2):H367-74.
698 46. Dekker RJ, van Soest S, Fontijn RD, Salamanca S, de Groot PG, VanBavel E, et
699 al. Prolonged fluid shear stress induces a distinct set of endothelial cell genes, most
700 specifically lung Kruppel-like factor (KLF2). Blood. 2002;100(5):1689-98.
701 47. Guo D, Chien S, Shyy JY. Regulation of endothelial cell cycle by laminar versus
702 oscillatory flow: distinct modes of interactions of AMP-activated protein kinase and Akt
703 pathways. Circ Res. 2007;100(4):564-71.
704 48. Coon BG, Timalsina S, Astone M, Zhuang ZW, Fang J, Han J, et al. A
705 mitochondrial contribution to anti-inflammatory shear stress signaling in vascular
706 endothelial cells. J Cell Biol. 2022;221(7).
707 49. Baeyens N, Larrivee B, Ola R, Hayward-Piatkowskyi B, Dubrac A, Huang B, et
708 al. Defective fluid shear stress mechanotransduction mediates hereditary hemorrhagic
709 telangiectasia. J Cell Biol. 2016;214(7):807-16.
710 50. Mack JJ, Mosqueiro TS, Archer BJ, Jones WM, Sunshine H, Faas GC, et al.
711 NOTCH1 is a mechanosensor in adult arteries. Nat Commun. 2017;8(1):1620.
712 51. Gallicchio M, Argyriou S, Ianches G, Filonzi EL, Zoellner H, Hamilton JA, et al.
713 Stimulation of PAI-1 expression in endothelial cells by cultured vascular smooth muscle
714 cells. Arterioscler Thromb. 1994;14(5):815-23.
715 52. Nackman GB, Bech FR, Fillinger MF, Wagner RJ, Cronenwett JL. Endothelial
716 cells modulate smooth muscle cell morphology by inhibition of transforming growth
717 factor-beta 1 activation. Surgery. 1996;120(2):418-25; discussion 25-6.

53. Powell RJ, Bhargava J, Basson MD, Sumpio BE. Coculture conditions alter endothelial modulation of TGF-beta 1 activation and smooth muscle growth morphology. Am J Physiol. 1998;274(2):H642-9.
54. Shirali AS, Romay MC, McDonald AI, Su T, Steel ME, Iruela-Arispe ML. A multi-step transcriptional cascade underlies vascular regeneration in vivo. Sci Rep. 2018;8(1):5430.
55. Boezio GL, Bensimon-Brito A, Piesker J, Guenther S, Helker CS, Stainier DY. Endothelial TGF-beta signaling instructs smooth muscle cell development in the cardiac outflow tract. Elife. 2020;9.
56. Birdsey GM, Dryden NH, Amsellem V, Gebhardt F, Sahnan K, Haskard DO, et al. Transcription factor Erg regulates angiogenesis and endothelial apoptosis through VE-cadherin. Blood. 2008;111(7):3498-506.
57. Laumonnier Y, Nadaud S, Agrapart M, Soubrier F. Characterization of an upstream enhancer region in the promoter of the human endothelial nitric-oxide synthase gene. J Biol Chem. 2000;275(52):40732-41.
58. Nikolova-Krstevski V, Yuan L, Le Bras A, Vijayaraj P, Kondo M, Gebauer I, et al. ERG is required for the differentiation of embryonic stem cells along the endothelial lineage. BMC Dev Biol. 2009;9:72.
59. Shah AV, Birdsey GM, Randi AM. Regulation of endothelial homeostasis, vascular development and angiogenesis by the transcription factor ERG. Vascul Pharmacol. 2016;86:3-13.
60. Yuan L, Nikolova-Krstevski V, Zhan Y, Kondo M, Bhasin M, Varghese L, et al. Antiinflammatory effects of the ETS factor ERG in endothelial cells are mediated through transcriptional repression of the interleukin-8 gene. Circ Res. 2009;104(9):1049-57.
61. Boquest AC, Shahdadfar A, Fronsdal K, Sigurjonsson O, Tunheim SH, Collas P, et al. Isolation and transcription profiling of purified uncultured human stromal stem cells: alteration of gene expression after in vitro cell culture. Mol Biol Cell. 2005;16(3):1131-41.
62. Bork S, Pfister S, Witt H, Horn P, Korn B, Ho AD, et al. DNA methylation pattern changes upon long-term culture and aging of human mesenchymal stromal cells. Aging Cell. 2010;9(1):54-63.
63. Forsyth NR, Kay A, Hampson K, Downing A, Talbot R, McWhir J. Transcriptome alterations due to physiological normoxic (2% O2) culture of human embryonic stem cells. Regen Med. 2008;3(6):817-33.
64. Roobrouck VD, Vanuytsel K, Verfaillie CM. Concise review: culture mediated changes in fate and/or potency of stem cells. Stem Cells. 2011;29(4):583-9.

764
765

Figure 1. Human umbilical cord endothelial cell transcriptome.
a. Model of endothelial cell collection for ex vivo (cord) and in vitro (culture) experiments. Endothelial cells are isolated in a slurry and used immediately for downstream experiments or cultured for subsequent passages. **b.** Principal component analysis (PCA) of transcriptome of the 7 matched cord, early culture and late culture samples with significant separation along PC1. **c.** Spearman-correlation demonstrating inter-condition (cord=C, early passage-=E, late passage=L) and intra sample variability with k-means clustering by cord **d.** 40-45% of the of the genes overlapped between cord and culture regardless of early and late culture. Early and late culture overlap in 93% of the genes. **e.** Volcano plot of genes most significantly expressed in cord (right) versus culture (left) by log10 fold change. **f.** Heatmap of top 30 differentially expressed genes in 21 samples from 7 individuals expressed between cord and culture **g.** Network profile of subset of GEOs significant in cord versus culture. GEO is represented by cluster identity and each term is represented as circle node visualized on Metascape. **h.** Mass spectrometry proteomic profile of 7 matched cord and culture separated by cord and culture on PC1 **i.** Scatter plot depicting RNA t-statistics (cord/culture) versus protein t-statistics (cord/culture) with a correlation coefficient of r=0.4.

Figure 2. Shear stress induces a time-dependent transcriptomic flow signature
a. Phenotype of *in vitro* flow model induces endothelial cellular shape changes under flow. **b.** PCA of static (red) versus flow induced endothelial cells by bulk RNA-seq **c.** Heatmap of bulk RNA-seq DEGs in static and control cells. Row z-score reflects the gene expression change. **d.** Volcano plot of statistical significance against fold change between flow and static culture demonstrating the most significantly differentially expressed genes. **e.** Time-dependent volcano plot and correlation coefficient demonstrating correlation of flow time to cord transcriptome where longer flow correlated more strongly to cord. **f.** Network profile of subset of GEOs significant in flow versus static culture. GEO is represented by cluster identity and each term is represented as circle node visualized on Metascape.

Figure 3. Flow rescues a degree of the cord transcriptome
a. PCA demonstrates flow rescuing culture signature across PC1. **b.** Venn-diagram demonstrating the significant number of differentially expressed genes by condition **c.** Correlation of top 10 module eigengenes (ME) with experimental conditions. The columns are labeled by experimental condition. The rows are labeled by the ME color. The biweight midcorrelation coefficients are shown for each cell, with the significance of the correlation shown immediately below (FDR). Cells are colorized based on the strength and sign of the correlation. **d.** Cluster dendrogram and module assignment for mRNA modules from WGCNA. Identification of gene co-expression modules using average hierarchical linkage clustering; the vertical axis denotes the co-expression distance and the horizontal axis corresponds to genes. Dynamic tree cutting was applied to identify modules by dividing the dendrogram at significant branch points. Modules are displayed with different colors in the horizontal bar immediately below the dendrogram, with gray representing unassigned genes. Correlation coefficients with experimental conditions are also represented based on strength and direction (negative correlations to positive correlations ranging from blue to red). **e-f.** Eigengene value of

flow-dependent rescue of the blue module; C=cord, E=early, L=late and enriched blue-module GEO. **g-h.** Eigengene value of flow-dependent rescue of the brown module and enriched GEO.

Figure 4. Endothelial cell-smooth muscle cell interactions

a. Schematic overview of single-cell RNAseq experiments. **b.** UMAP of single cell gene expression demonstrating four distinct clusters with 2 technical replicates (labeled A/B) in the legend with confirmation of endothelial identity by UMAP of CDH5 and PECAM1 on the right. **c.** Confirming endothelial cell identity by CDH5 and PECAM positive staining in endothelial cell specific clusters. **d.** Heatmap identifying most highly differentially expressed genes with log fold>2 for each condition relative to the other cell types. **e.** Ingenuity analysis demonstrates most significantly upregulated module score based on growth factors, cytokines, and transcription factors. **f.** TGFB1 and VEGF have the highest module score in co-culture relative to endothelial cell monoculture **i.** TGFB1 family members are upregulated in co-culture **j.** Clathrin family members are upregulated in co-culture; whereas caveolin family members are decreased in co-culture **k.** Endothelial cell makers are unchanged and stable in mono- and co-culture endothelial cells

Figure 5. Co-cultured endothelial cells rescue the cord transcriptome

a. UMAP of endothelial cell co-culture (EC-CC) with smooth muscle cells versus endothelial cell-monoculture (EC-MC) recovers some degree of the cord transcriptome as demonstrated by scRNAseq. Insert: confirmed endothelial cell identity by PECAM positive cells. **b.** Ingenuity analysis demonstrates most significantly upregulated module score based on growth factors, cytokines, and transcription factors. **c.** PDGFB, the most significantly upregulated growth factor, is rescued in co-culture. **d.** Environment dependent transcriptional enrichment demonstrated by UMAP. **e.** Dotpolot demonstrates the top markers of in cord, monoculture (MC), and co-culture (CC). Dot size corresponds to the proportion of cells within the group expressing each transcript and dot color intensity corresponds to the expression level. **f.** Violin plot of environment dependent gene expression defines

Figure 6. Summary Figure. Schematic representing experimental design, culture conditions, and corresponding validated genes changes.

FIGURE 1

Afshar Y, *et. al.*

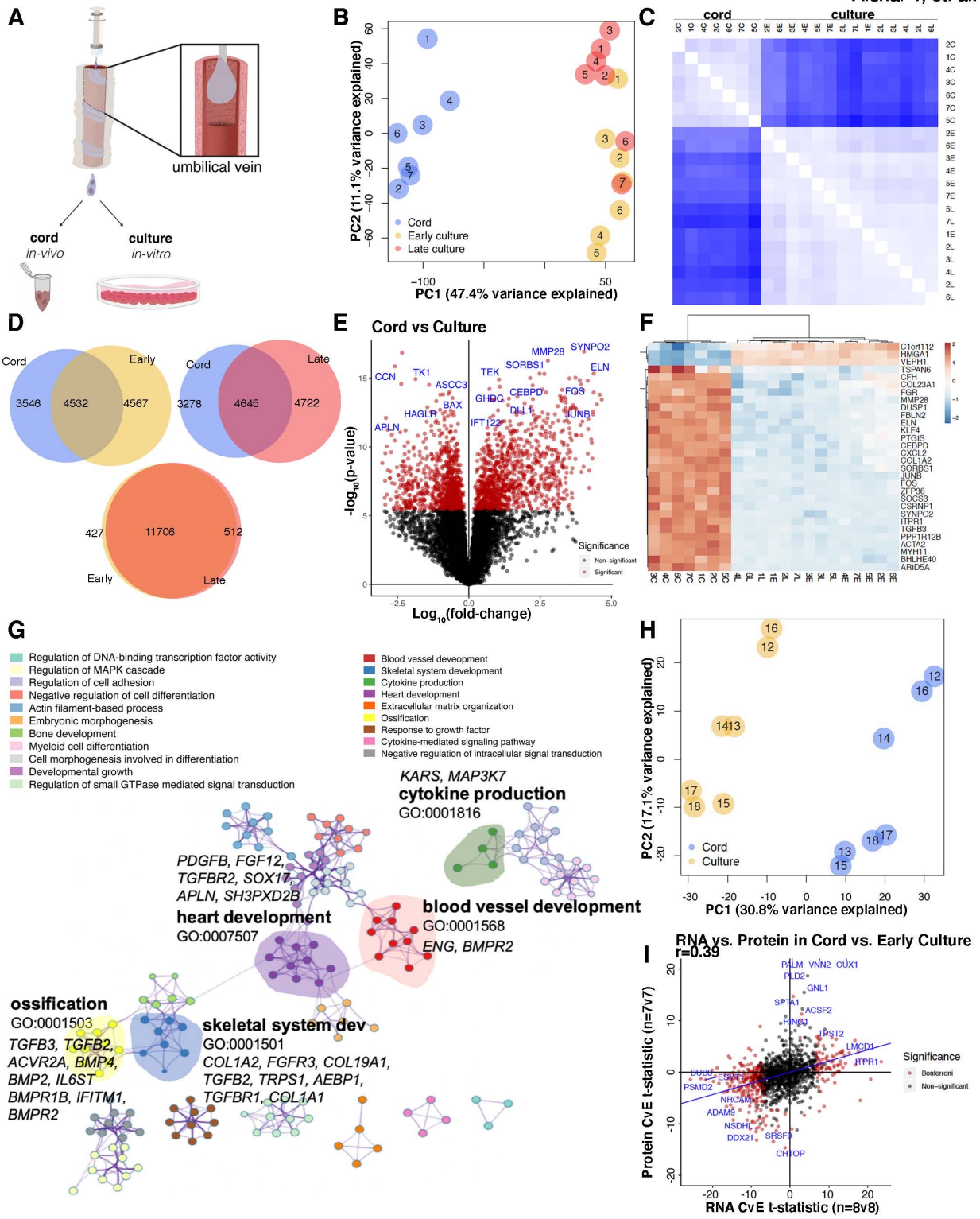

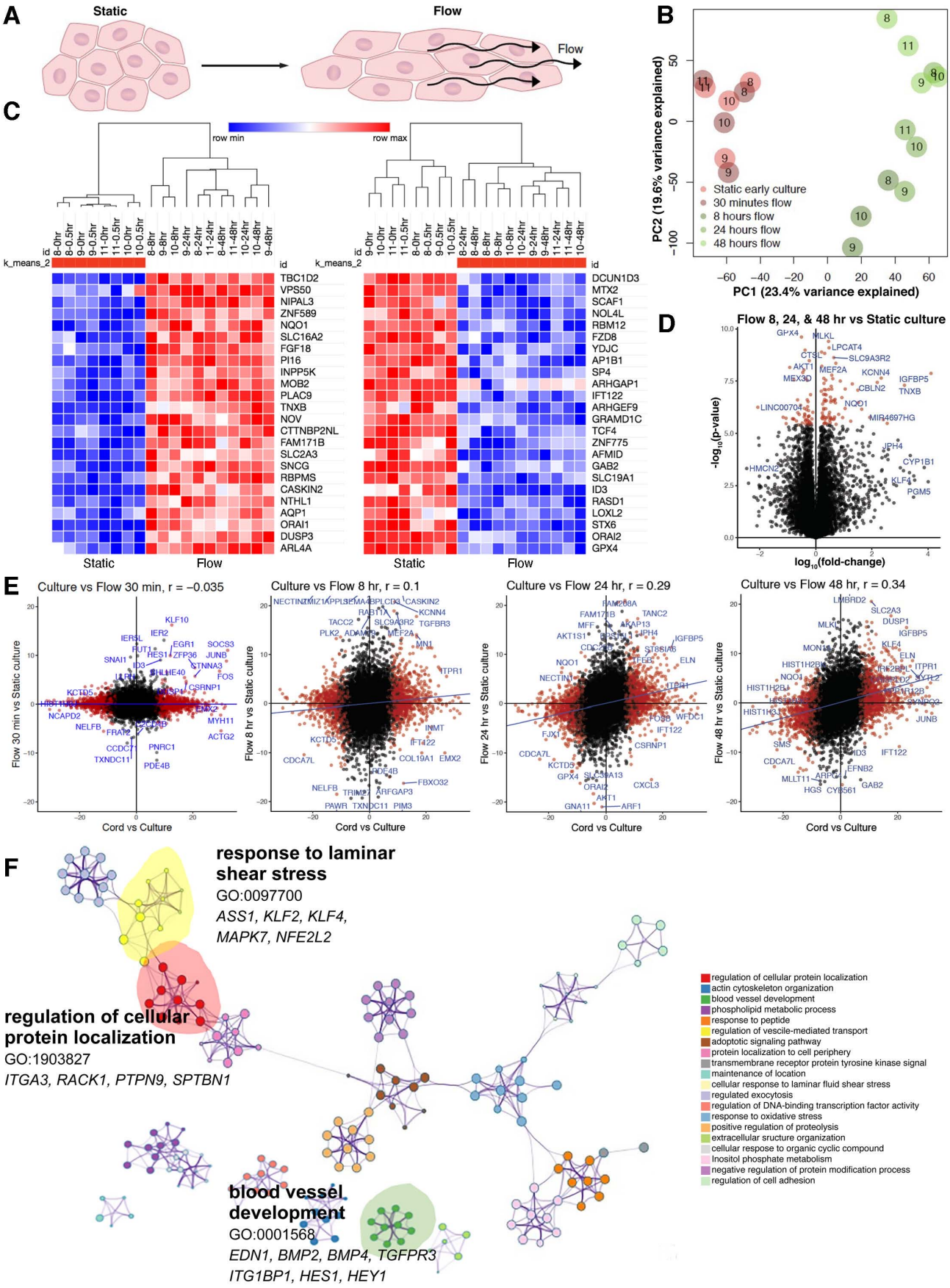
A
Static
Flow
Flow
B
PC2 (19.6% variance explained)
PC1 (23.4% variance explained)
Static early culture
30 minutes flow
8 hours flow
24 hours flow
48 hours flow
C
row min
row max
k_means_2
id
TBC1D2
VPS50
NIPAL3
ZNF589
NQO1
SLC16A2
FGF18
PI16
INPP5K
MOB2
PLAC9
TNXB
NOV
CTTNBP2NL
FAM171B
SLC2A3
SNCG
RBPMS
CASKIN2
NTHL1
AQP1
ORAI1
DUSP3
ARL4A
DCUN1D3
MTX2
SCAF1
NOL4L
RBM12
FZD8
YDJC
AP1B1
SP4
ARHGAP1
IFT122
ARHGEF9
GRAMD1C
TCF4
ZNF775
AFMID
GAB2
SLC19A1
ID3
RASD1
LOXL2
STX6
ORAI2
GPX4
Static
Flow
D
Flow 8, 24, & 48 hr vs Static culture
-log10(p-value)
log10(fold-change)
E
Culture vs Flow 30 min, r = −0.035
Culture vs Flow 8 hr, r = 0.1
Culture vs Flow 24 hr, r = 0.29
Culture vs Flow 48 hr, r = 0.34
Flow 30 min vs Static culture
Flow 8 hr vs Static culture
Flow 24 hr vs Static culture
Flow 48 hr vs Static culture
Cord vs Culture
F
response to laminar shear stress
GO:0097700
ASS1, KLF2, KLF4, MAPK7, NFE2L2
regulation of cellular protein localization
GO:1903827
ITGA3, RACK1, PTPN9, SPTBN1
blood vessel development
GO:0001568
EDN1, BMP2, BMP4, TGFPR3
ITG1BP1, HES1, HEY1
regulation of cellular protein localization
actin cytoskeleton organization
blood vessel development
phospholipid metabolic process
response to peptide
regulation of vesicle-mediated transport
adoptotic signaling pathway
protein localization to cell periphery
transmembrane receptor protein tyrosine kinase signal
maintenance of location
cellular response to laminar fluid shear stress
regulated exocytosis
regulation of DNA-binding transcription factor activity
response to oxidative stress
positive regulation of proteolysis
extracellular sructure organization
cellular respose to organic cyclic compound
Inositol phosphate metabolism
negative regulation of protein modification process
regulation of cell adhesion

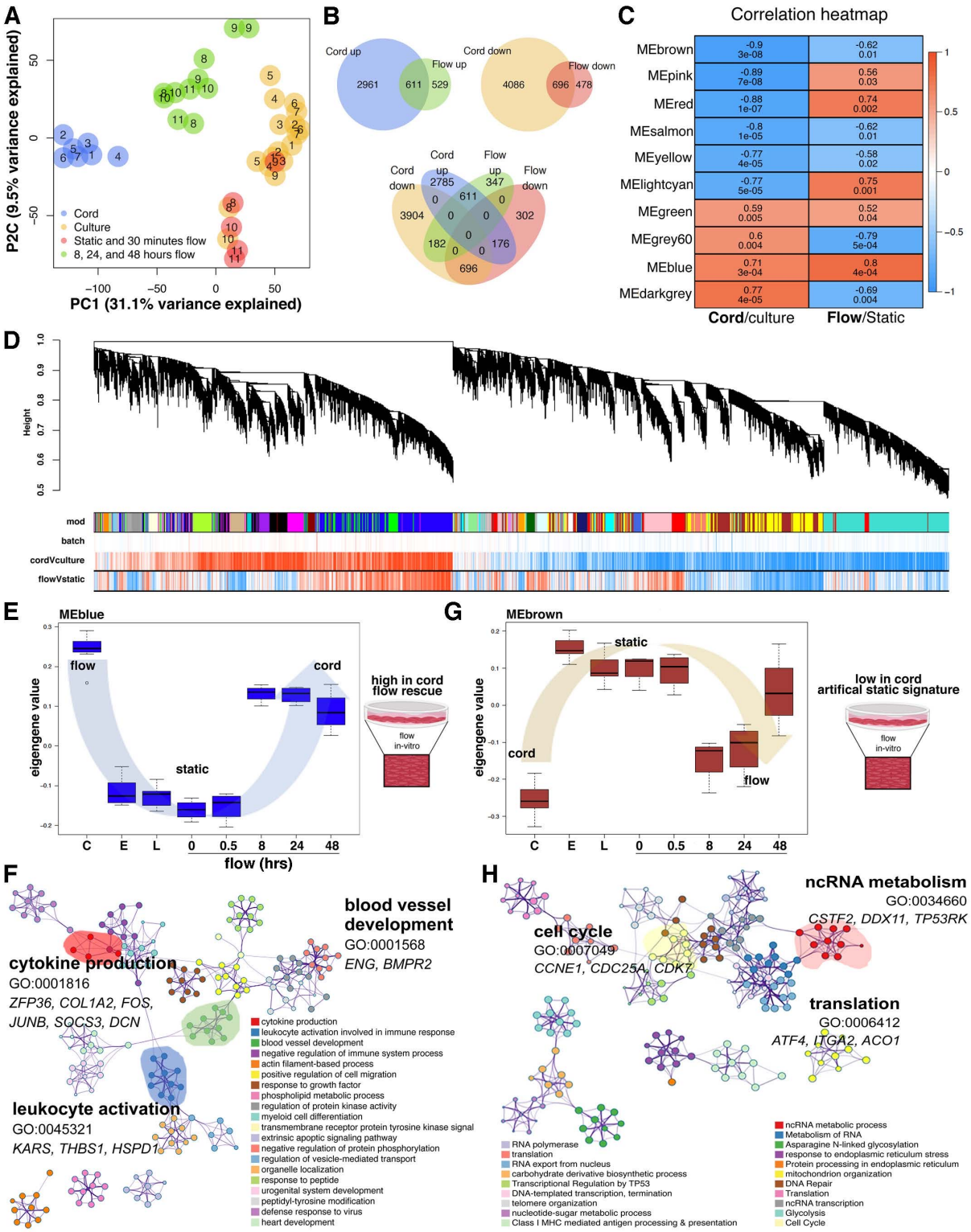
A
P2C (9.5% variance explained)
PC1 (31.1% variance explained)
Cord
Culture
Static and 30 minutes flow
8, 24, and 48 hours flow
B
Cord up
Flow up
Cord down
Flow down
2961
611
529
4086
696
478
Cord up
Flow up
Cord down
Flow down
2785
347
3904
302
611
182
176
696
C
Correlation heatmap
MEbrown
MEpink
MEred
MEsalmon
MEyellow
MElightcyan
MEgreen
MEgrey60
MEblue
MEdarkgrey
-0.9 3e-08
-0.62 0.01
-0.89 7e-08
0.56 0.03
-0.88 1e-07
0.74 0.002
-0.8 1e-05
-0.62 0.01
-0.77 4e-05
-0.58 0.02
-0.77 5e-05
0.75 0.001
0.59 0.005
0.52 0.04
0.6 0.004
-0.79 5e-04
0.71 3e-04
0.8 4e-04
0.77 4e-05
-0.69 0.004
Cord/culture
Flow/Static
D
Height
mod
batch
cordVculture
flowVstatic
E
MEblue
eigengene value
flow
cord
static
C E L 0 0.5 8 24 48
flow (hrs)
high in cord
flow rescue
flow in-vitro
G
MEbrown
eigengene value
static
cord
flow
C E L 0 0.5 8 24 48
low in cord
artifical static signature
flow in-vitro
F
blood vessel development
GO:0001568
ENG, BMPR2
cytokine production
GO:0001816
ZFP36, COL1A2, FOS, JUNB, SOCS3, DCN
leukocyte activation
GO:0045321
KARS, THBS1, HSPD1
cytokine production
leukocyte activation involved in immune response
blood vessel development
negative regulation of immune system process
actin filament-based process
positive regulation of cell migration
response to growth factor
phospholipid metabolic process
regulation of protein kinase activity
myeloid cell differentiation
transmembrane receptor protein tyrosine kinase signal
extrinsic apoptic signaling pathway
negative regulation of protein phosphorylation
regulation of vesicle-mediated transport
organelle localization
response to peptide
urogenital system development
peptidyl-tyrosine modification
defense response to virus
heart development
H
ncRNA metabolism
GO:0034660
CSTF2, DDX11, TP53RK
cell cycle
GO:0007049
CCNE1, CDC25A, CDK7
translation
GO:0006412
ATF4, ITGA2, ACO1
RNA polymerase
translation
RNA export from nucleus
carbohydrate derivative biosynthetic process
Transcriptional Regulation by TP53
DNA-templated transcription, termination
telomere organization
nucleotide-sugar metabolic process
Class I MHC mediated antigen processing & presentation
ncRNA metabolic process
Metabolism of RNA
Asparagine N-linked glycosylation
response to endoplasmic reticulum stress
Protein processing in endoplasmic reticulum
mitochondrion organization
DNA Repair
Translation
ncRNA transcription
Glycolysis
Cell Cycle

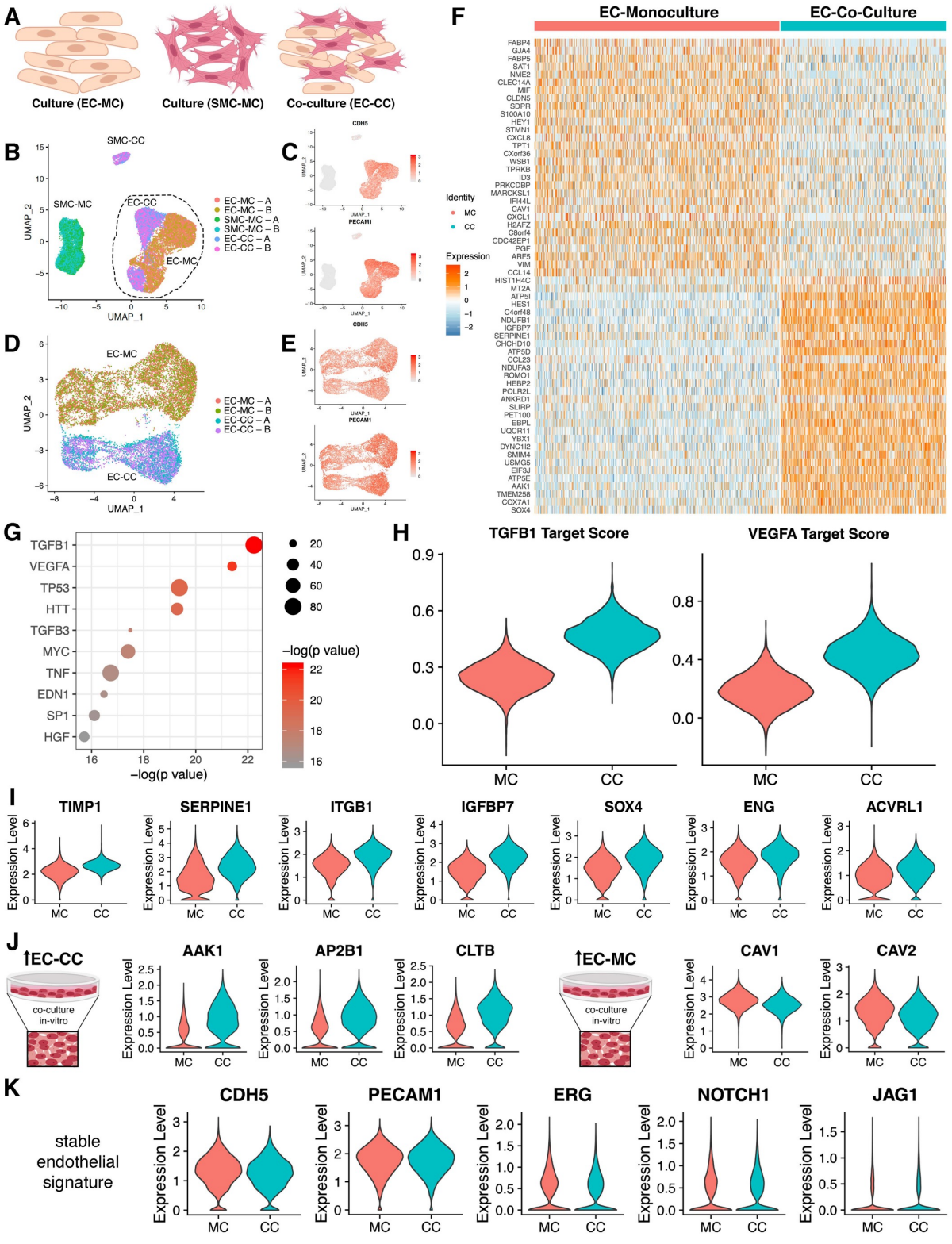
A
Culture (EC-MC)
Culture (SMC-MC)
Co-culture (EC-CC)
B
SMC-CC
SMC-MC
EC-CC
EC-MC
EC-MC – A
EC-MC – B
SMC-MC – A
SMC-MC – B
EC-CC – A
EC-CC – B
UMAP_1
UMAP_2
C
CDH5
PECAM1
D
E
F
EC-Monoculture
EC-Co-Culture
Identity
MC
CC
Expression
G
TGFB1
VEGFA
TP53
HTT
TGFB3
MYC
TNF
EDN1
SP1
HGF
–log(p value)
H
TGFB1 Target Score
VEGFA Target Score
MC
CC
I
TIMP1
SERPINE1
ITGB1
IGFBP7
SOX4
ENG
ACVRL1
Expression Level
J
↑EC-CC
co-culture in-vitro
AAK1
AP2B1
CLTB
↑EC-MC
CAV1
CAV2
K
stable endothelial signature
CDH5
PECAM1
ERG
NOTCH1
JAG1

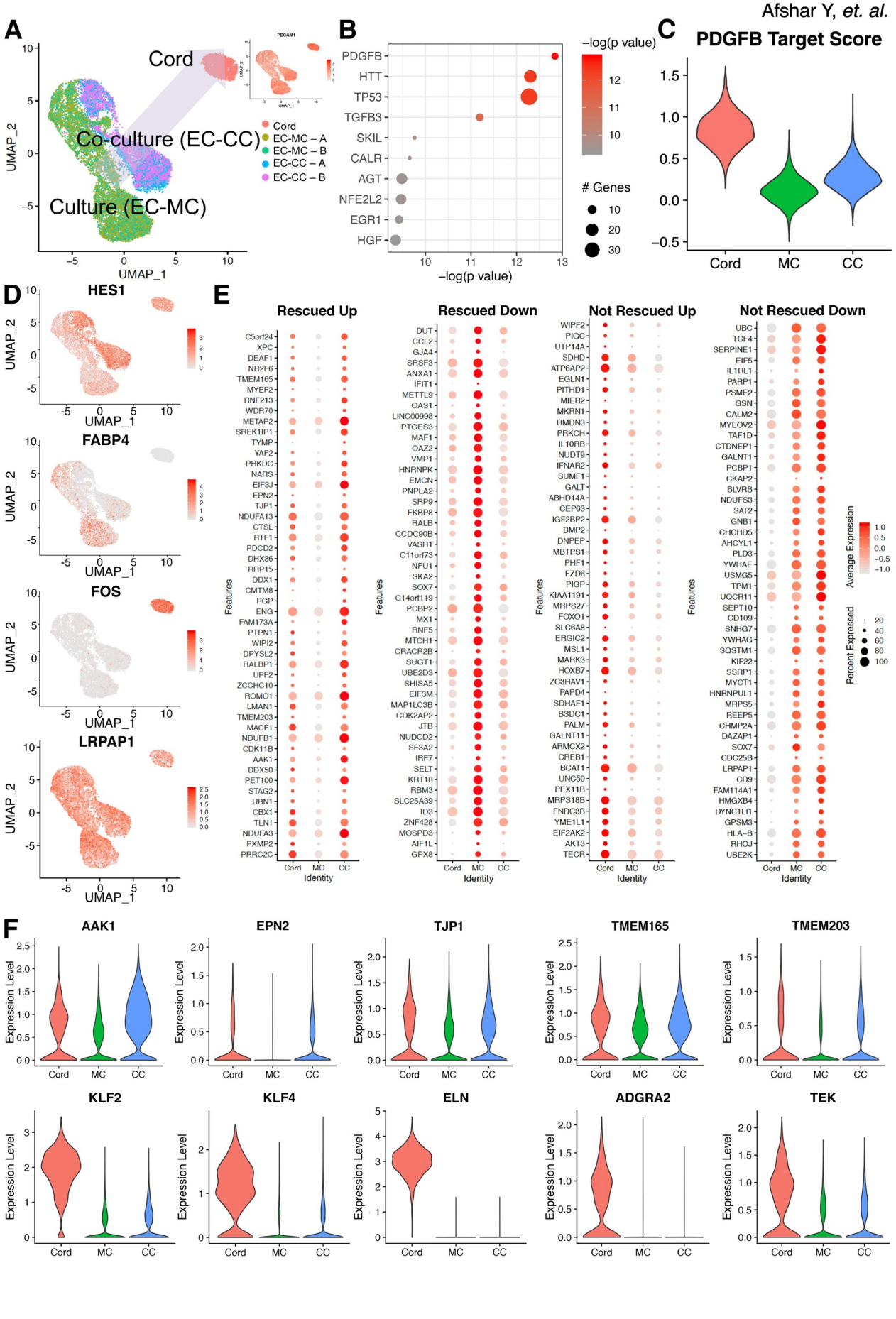
A
Cord
Co-culture (EC-CC)
Culture (EC-MC)
PECAM1
Cord
EC-MC – A
EC-MC – B
EC-CC – A
EC-CC – B
UMAP_1
UMAP_2
B
PDGFB
HTT
TP53
TGFB3
SKIL
CALR
AGT
NFE2L2
EGR1
HGF
−log(p value)
Genes
C
PDGFB Target Score
Cord
MC
CC
D
HES1
FABP4
FOS
LRPAP1
E
Rescued Up
Rescued Down
Not Rescued Up
Not Rescued Down
Features
Identity
Average Expression
Percent Expressed
F
AAK1
EPN2
TJP1
TMEM165
TMEM203
KLF2
KLF4
ELN
ADGRA2
TEK
Expression Level

FIGURE 6
Afshar Y, *et al*

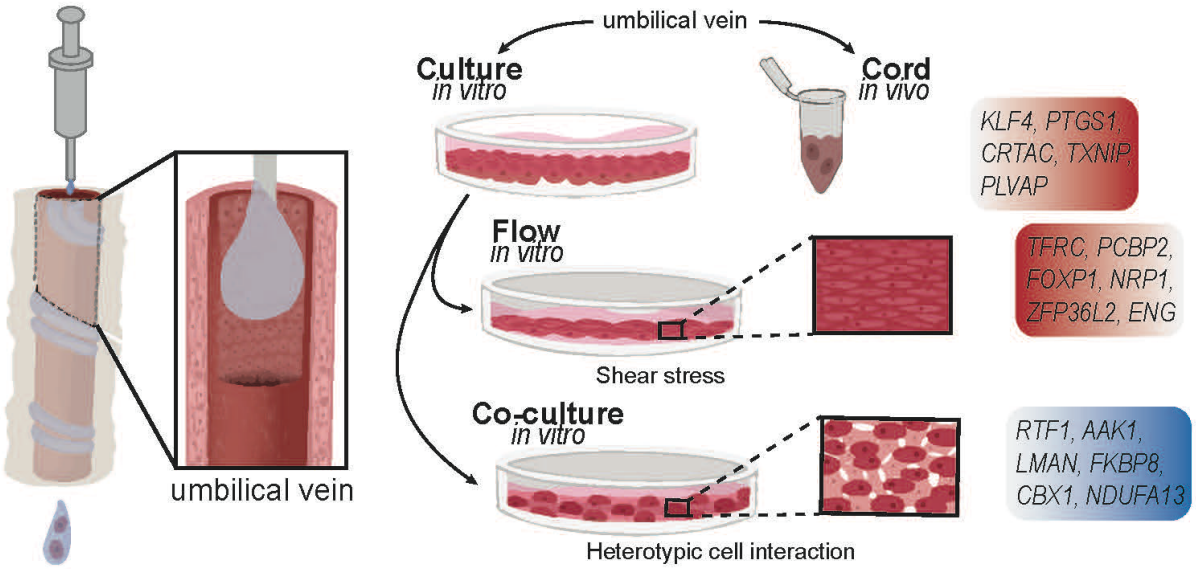

Table 1. Patient Demographics

	Sample Code	Gestational Age	Fetal Sex	Race
Bulk RNAseq				
cord, early culture p2-3, and late culture p7-8 experiments	1	40w1d	M	Asian, Vietnamese
	2	39w4d	F	Asian, Chinese
	3	39w4d	M	Asian
	4	39w1d	M	Asian
	5	39w0d	F	White
	6	37w5d	M	White
	7	38w4d	F	White
Flow, RNASeq				
culture static versus culture flow experiments	8	39w6d	F	White
	9	40w5d	F	Black
	10	40w4d	F	Asian, Chinese
	11	39w5d	M	White
Proteomics				
cord versus culture experiments	12	40w2d	M	Asian, Indian
	13	39w3d	F	Latino
	14	37w2d	M	Latino
	15	39w3d	M	Asian, Chinese
	16	38w5d	F	Latino
	17	37w0d	M	Asian, Other
	18	40w0d	F	White
ATACseq				
cord versus culture experiments	19	40w2d	M	Latino
	20	37w2d	M	American Indian/Alaska Native
	21	37w6d	M	White
	22	41w2d	M	White
	23	38w3d	M	White
scRNAseq				
culture (monoculture) versus co-culture experiments	SMC	37w3d	F	Latino (Other)
	EC	36w4d	M	Other

Table 2. Upregulated and Downregulated Transcripts: Cord and Flow

Cord Up		Cord Down		Flow Up		Flow Down	
gene	t-statistic	gene	t-statistic	gene	t-statistic	gene	t-statistic
PPP1R12B	36.58	CCNB2	-33.05	SLC9A3R2	17.50	KIT	-16.51
SYNPO2	36.36	CCNA2	-28.22	CMKLR1	15.49	TNFRSF21	-15.17
FOS	33.43	SMS	-26.62	NDRG1	15.22	CDCA7L	-13.59
JUNB	32.91	VEPH1	-25.14	IGFBP5	14.14	PDGFB	-11.33
SOCS3	30.80	CENPO	-24.67	ADAMTS1	13.64	SLC7A7	-11.28
ITPR1	30.77	POLH	-24.52	HSPA12B	13.57	ACSS1	-11.08
ACTA2	28.94	CEP55	-24.17	AL365205.1	13.43	PIM3	-11.05
TGFB3	27.66	TK1	-24.15	CYP1B1	13.41	COLEC12	-10.83
SYTL2	26.96	HMGA2	-23.57	TBC1D2	13.28	TCF4	-10.76
BMP6	26.86	KIFC1	-22.98	COL17A1	12.89	CYTOR	-10.70
CRISPLD2	26.40	RRM2	-22.21	LAMB3	12.43	RASD1	-10.67
SORBS1	26.32	LINC01013	-21.91	PLPP3	12.33	CHST15	-10.26
MMP28	25.97	FEN1	-21.55	KLF8	11.83	EVA1A	-10.09
SLC41A3	25.73	NCAPD2	-21.46	ST8SIA6	11.72	RALGPS2	-10.06
CEBPD	24.98	FJX1	-21.45	KCNN4	11.70	VASH1	-10.02
ELN	24.54	PRR11	-21.33	TANC2	11.65	TGFBRAP1	-9.73
FGF18	24.32	CDCA7L	-20.93	CCM2L	11.37	FILIP1	-9.71
FOSB	24.23	UHRF1	-20.83	HEG1	11.30	PAWR	-9.58
ZFP36	24.06	KPNB1	-20.72	JPH4	11.24	ARID3A	-9.40
CXCL2	23.80	PIMREG	-20.70	CDC25B	11.07	FZD8	-9.33
C6orf89	23.21	HMGA1	-20.66	RAPGEF5	11.01	SEC14L1	-9.14
ID2	22.86	CDCA2	-20.66	PLAC9	10.78	AMOTL2	-9.10
ATF3	22.76	MDM2	-20.56	S100A4	10.54	FGD4	-9.04
MTURN	22.53	HIST1H2AG	-20.56	MYOM3	10.52	OSBPL10	-9.01
CMKLR1	22.34	C19orf48	-20.50	PTHLH	10.45	PDE4B	-8.96
FNIP2	22.28	ADK	-20.43	CCDC69	10.44	ABCA6	-8.93
IGFBP5	22.27	HIST1H2BN	-20.06	NOV	10.27	GRAMD1C	-8.92
KLF4	22.12	PSMD2	-19.76	KIAA1522	10.10	DACH1	-8.72
FBLN2	22.01	TPX2	-19.57	ATP1A1	9.62	C15orf54	-8.71

Table 3. Concordance and Discordance of Transcripts with Flow (vs Cord)

Cord and Flow UP		Cord and Flow DOWN		Cord UP : Flow DOWN		Cord DOWN : Flow UP	
gene	t-statistic	gene	t-statistic	gene	t-statistic	gene	t-statistic
ITPR1	30.77	SMS	-26.62	JUNB	32.91	HIST1H2AG	-20.56
ACTA2	28.94	VEPH1	-25.14	BMP6	26.86	NQO1	-16.83
SYTL2	26.96	HMGA2	-23.57	ZFP36	24.06	TMEM171	-14.80
CRISPLD2	26.40	LINC01013	-21.91	ID2	22.86	HIST1H2BJ	-14.35
CEBPD	24.98	FEN1	-21.55	CCDC80	20.75	EFNB1	-13.85
ELN	24.54	FJX1	-21.45	ARHGEF9	18.92	HIST1H2BK	-12.60
FGF18	24.32	CDCA7L	-20.93	CXCL3	18.37	NECTIN1	-12.54
MTURN	22.53	UHRF1	-20.83	CSRNP1	18.14	HIST1H3H	-12.24
CMKLR1	22.34	HMGA1	-20.66	HMCN2	17.38	AKR1B1	-12.22
FNIP2	22.28	C19orf48	-20.50	GPR146	16.22	SCARB1	-11.47
IGFBP5	22.27	MAP4K4	-18.92	IFT122	16.05	SPATA18	-11.22
KLF4	22.12	DKK1	-18.48	FAT4	15.64	STRIP2	-11.05
FBLN2	22.01	UBE2S	-18.06	SIRPB2	15.39	ZNF185	-10.99
TEK	21.60	SLC1A1	-17.71	MKL2	15.38	HIST1H4H	-10.47
NEO1	21.46	SNRPA	-17.39	GABARAPL1	15.21	CAPN2	-9.73
DUSP1	21.34	SAE1	-17.35	VWF	14.97	OSGIN1	-9.64
ITGA1	21.25	APLN	-17.19	PPP1R15A	14.71	AC005699.1	-9.58
RAMP2	20.74	CFL1	-17.10	INTU	14.58	TKT	-9.49
NTN1	20.34	FGF16	-16.86	CTSO	14.39	CCDC34	-9.43
AQP1	20.32	CDK2AP1	-16.69	CACNA1H	14.33	RCC1	-9.41
LYST	20.05	NME4	-16.21	EGR1	14.27	MIR34AHG	-8.97
SRL	19.72	GAS2L3	-16.17	FBXO32	14.17	LYAR	-8.73
SLC22A4	19.61	ARHGAP18	-15.80	PGAP3	14.05	HIST1H2BC	-8.53
MMP24	19.61	CENPN	-15.62	CYP27A1	13.89	LRRC8D	-8.45
RAPGEF4	19.36	RALA	-15.26	OLFML3	13.58	ADGRG1	-8.26
PLCB4	19.22	ARHGAP24	-15.13	GUCY1A2	13.57	PHLDA3	-8.23
KCNN3	19.01	PFN1	-14.99	CDKN1C	13.53	SYNJ2	-8.21
JPH4	18.95	LMNB2	-14.72	ATRN	13.40	PLAT	-8.13
TGFBR3	18.95	NACC1	-14.69	RAB11FIP1	13.36	HIST1H2BE	-8.04

SUPPLEMENTAL FIGURES

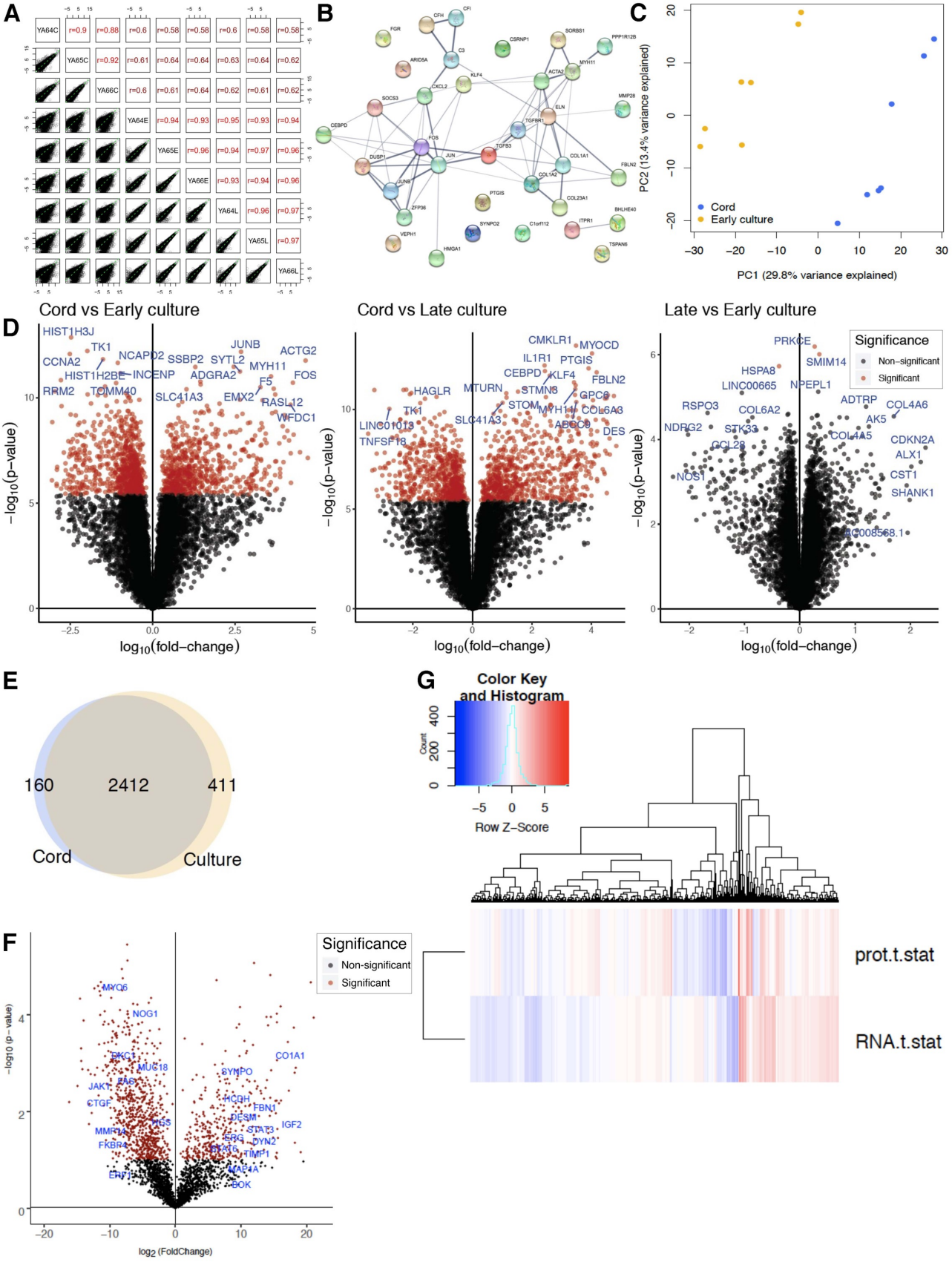
A
YA64C
YA65C
YA66C
YA64E
YA65E
YA66E
YA64L
YA65L
YA66L
B
C
PC2 (13.4% variance explained)
PC1 (29.8% variance explained)
Cord
Early culture
D
Cord vs Early culture
Cord vs Late culture
Late vs Early culture
−log10(p−value)
log10(fold−change)
Significance
Non−significant
Significant
E
160
2412
411
Cord
Culture
F
log2 (FoldChange)
G
Color Key and Histogram
Count
Row Z−Score
prot.t.stat
RNA.t.stat

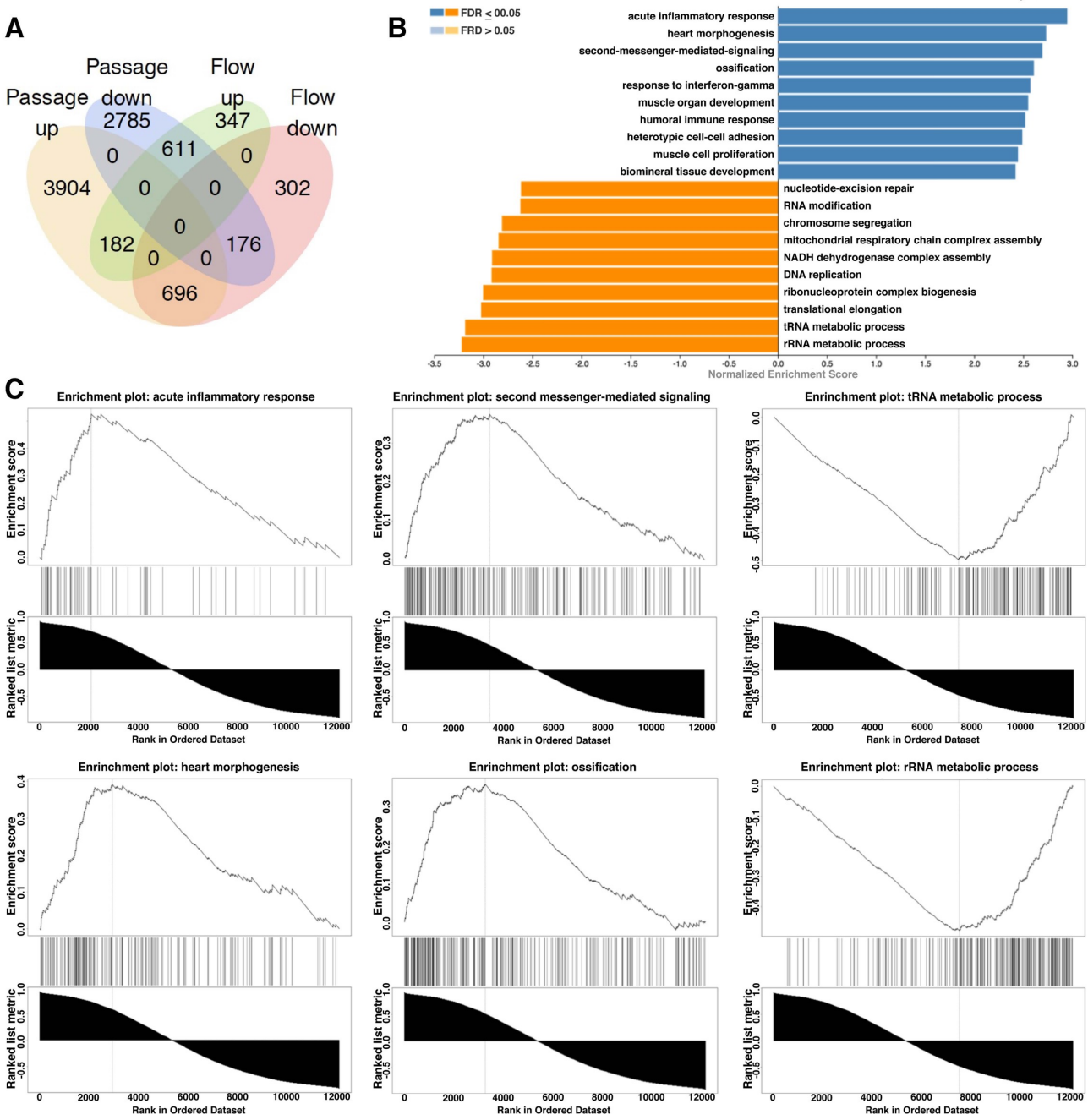
A
Passage up
Passage down
Flow up
Flow down
2785
347
302
3904
611
0
0
0
0
182
176
0
0
696
B
FDR ≤ 00.05
FRD > 0.05
acute inflammatory response
heart morphogenesis
second-messenger-mediated-signaling
ossification
response to interferon-gamma
muscle organ development
humoral immune response
heterotypic cell-cell adhesion
muscle cell proliferation
biomineral tissue development
nucleotide-excision repair
RNA modification
chromosome segregation
mitochondrial respiratory chain complrex assembly
NADH dehydrogenase complex assembly
DNA replication
ribonucleoprotein complex biogenesis
translational elongation
tRNA metabolic process
rRNA metabolic process
Normalized Enrichment Score
C
Enrichment plot: acute inflammatory response
Enrichment plot: second messenger-mediated signaling
Enrichment plot: tRNA metabolic process
Enrichment plot: heart morphogenesis
Enrichment plot: ossification
Enrichment plot: rRNA metabolic process
Enrichment score
Ranked list metric
Rank in Ordered Dataset
D
Flow 30 min vs Static culture
Flow 8 hr vs Static culture
Flow 24 hr vs Static culture
Flow 48 hr vs Static culture
−log10(p−value)
log10(fold−change)

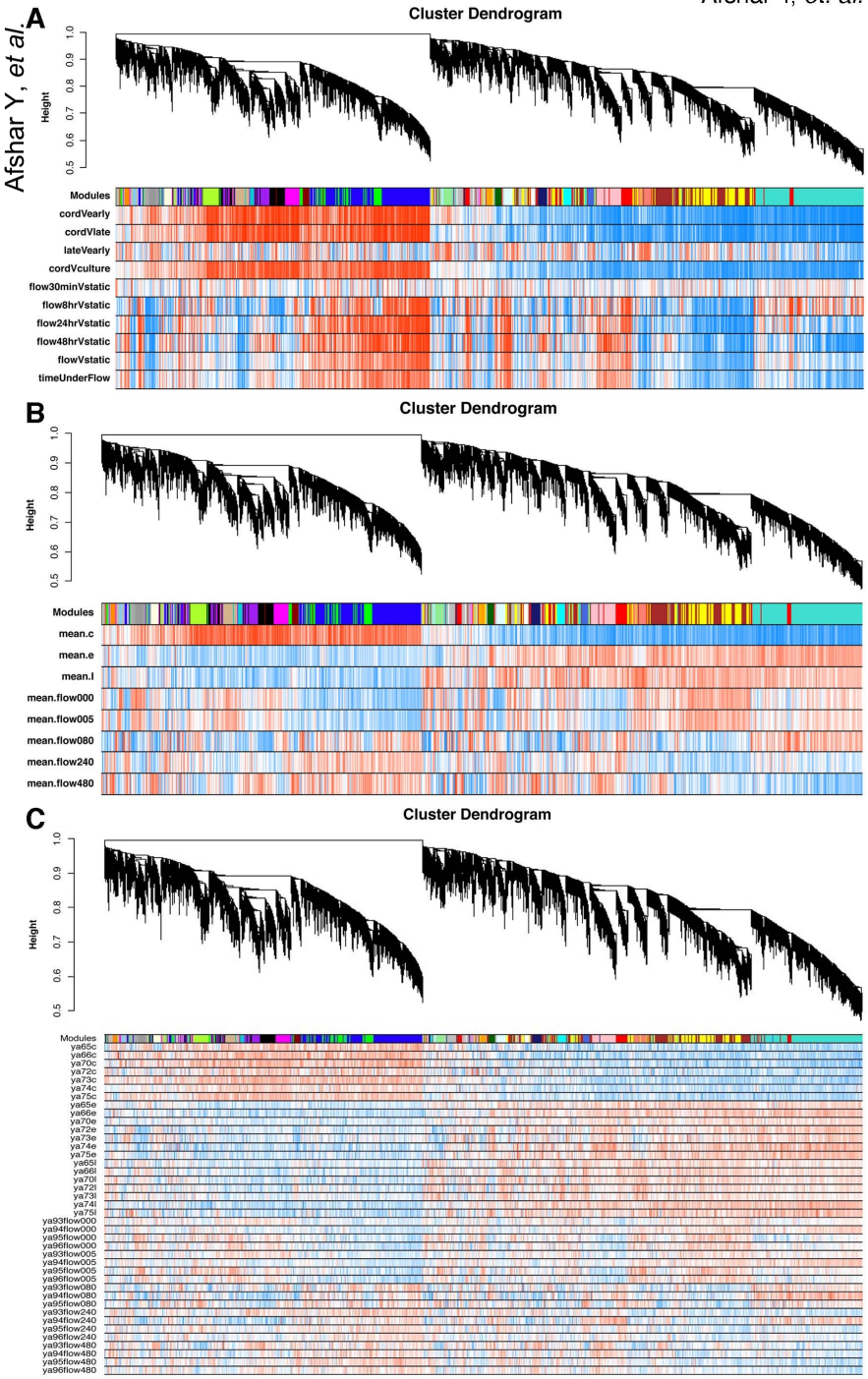
A
Cluster Dendrogram
Height
Modules
cordVearly
cordVlate
lateVearly
cordVculture
flow30minVstatic
flow8hrVstatic
flow24hrVstatic
flow48hrVstatic
flowVstatic
timeUnderFlow
B
Cluster Dendrogram
Height
Modules
mean.c
mean.e
mean.l
mean.flow000
mean.flow005
mean.flow080
mean.flow240
mean.flow480
C
Cluster Dendrogram
Height
Modules

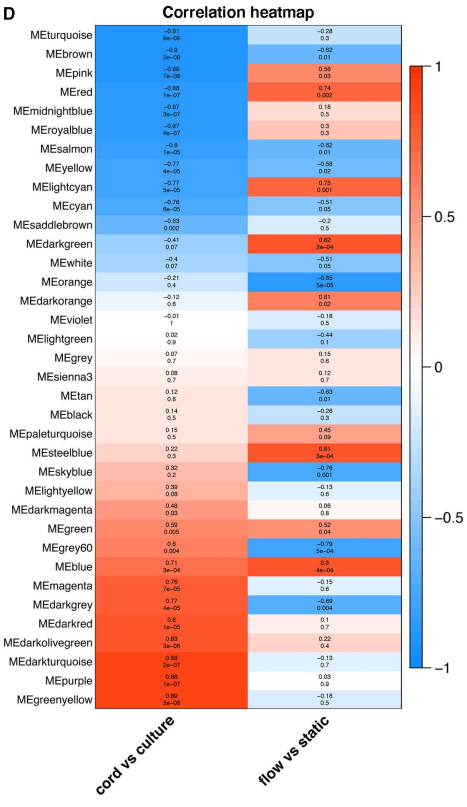
D
Correlation heatmap
MEturquoise
MEbrown
MEpink
MEred
MEmidnightblue
MEroyalblue
MEsalmon
MEyellow
MElightcyan
MEcyan
MEsaddlebrown
MEdarkgreen
MEwhite
MEorange
MEdarkorange
MEviolet
MElightgreen
MEgrey
MEsienna3
MEtan
MEblack
MEpaleturquoise
MEsteelblue
MEskyblue
MElightyellow
MEdarkmagenta
MEgreen
MEgrey60
MEblue
MEmagenta
MEdarkgrey
MEdarkred
MEdarkolivegreen
MEdarkturquoise
MEpurple
MEgreenyellow
1
0.5
0
−0.5
−1
cord vs culture
flow vs static

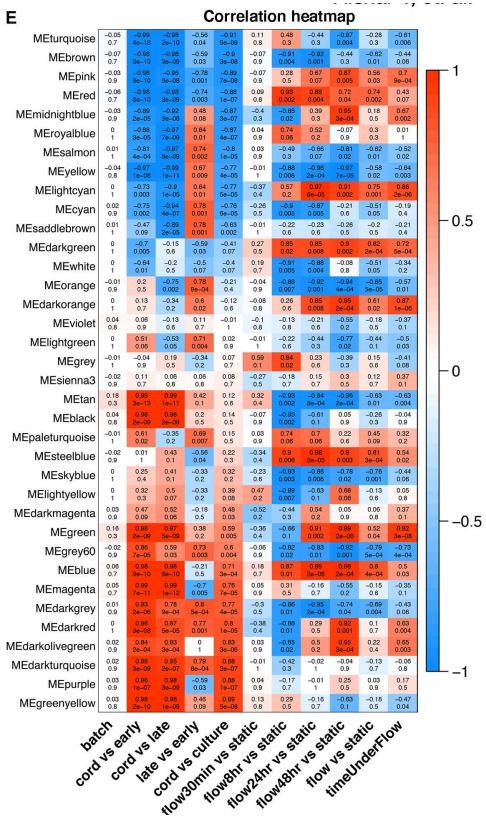
E
Correlation heatmap
MEturquoise
MEbrown
MEpink
MEred
MEmidnightblue
MEroyalblue
MEsalmon
MEyellow
MElightcyan
MEcyan
MEsaddlebrown
MEdarkgreen
MEwhite
MEorange
MEdarkorange
MEviolet
MElightgreen
MEgrey
MEsienna3
MEtan
MEblack
MEpaleturquoise
MEsteelblue
MEskyblue
MElightyellow
MEdarkmagenta
MEgreen
MEgrey60
MEblue
MEmagenta
MEdarkgrey
MEdarkred
MEdarkolivegreen
MEdarkturquoise
MEpurple
MEgreenyellow
1
0.5
0
−0.5
−1
batch
cord vs early
cord vs late
late vs early
cord vs culture
flow30min vs static
flow8hr vs static
flow24hr vs static
flow48hr vs static
flow vs static
timeUnderFlow

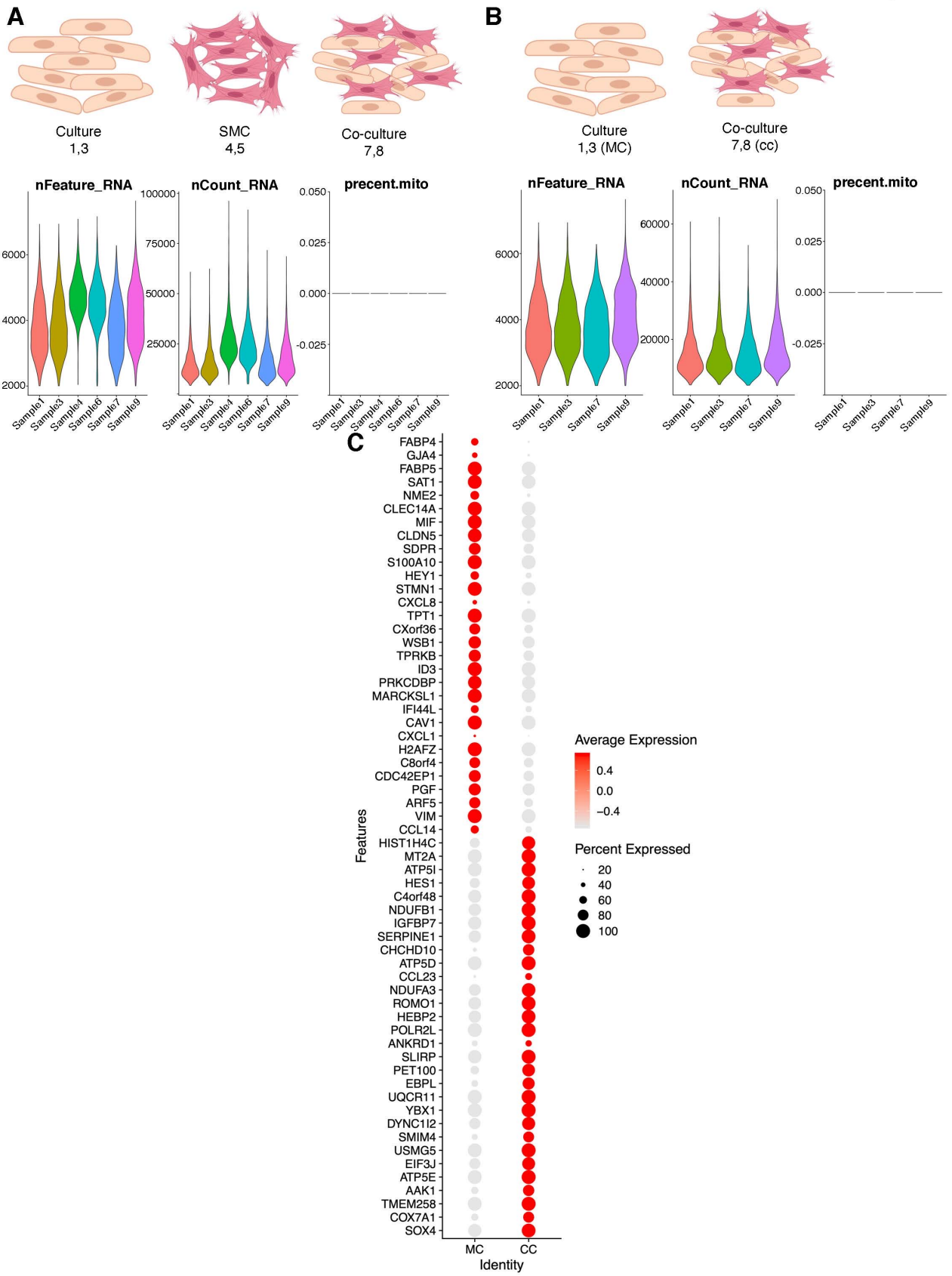
A
Culture
1,3
SMC
4,5
Co-culture
7,8
nFeature_RNA
nCount_RNA
precent.mito
Sample1
Sample3
Sample4
Sample6
Sample7
Sample9
B
Culture
1,3 (MC)
Co-culture
7,8 (cc)
C
FABP4
GJA4
FABP5
SAT1
NME2
CLEC14A
MIF
CLDN5
SDPR
S100A10
HEY1
STMN1
CXCL8
TPT1
CXorf36
WSB1
TPRKB
ID3
PRKCDBP
MARCKSL1
IFI44L
CAV1
CXCL1
H2AFZ
C8orf4
CDC42EP1
PGF
ARF5
VIM
CCL14
HIST1H4C
MT2A
ATP5I
HES1
C4orf48
NDUFB1
IGFBP7
SERPINE1
CHCHD10
ATP5D
CCL23
NDUFA3
ROMO1
HEBP2
POLR2L
ANKRD1
SLIRP
PET100
EBPL
UQCR11
YBX1
DYNC1I2
SMIM4
USMG5
EIF3J
ATP5E
AAK1
TMEM258
COX7A1
SOX4
Features
MC
CC
Identity
Average Expression
0.4
0.0
−0.4
Percent Expressed
20
40
60
80
100